Numerische Mathematik

Numerical solution of a bending-torsion model for elastic rods

Sören Bartels[1] · Philipp Reiter[2]

Abstract

Aiming at simulating elastic rods, we discretize a rod model based on a general theory of hyperelasticity for inextensible and unshearable rods. After reviewing this model and discussing topological effects of periodic rods, we prove convergence of the discretized functionals and stability of a corresponding discrete flow. Our experiments numerically confirm thresholds, e.g., for Michell's instability, and indicate a complex energy landscape, in particular in the presence of impermeability.

Contents

1 Introduction

Long slender objects—such as springy wires made of plastic or metal—can be approximated by curves. In many cases, equilibrium shapes are characterized in terms of the

✉ Sören Bartels
bartels@mathematik.uni-freiburg.de

Philipp Reiter
philipp.reiter@mathematik.uni-halle.de

1 Abteilung für Angewandte Mathematik, Albert-Ludwigs-Universität Freiburg,
Hermann-Herder-Str. 10, 79104 Freiburg im Breisgau, Germany

2 Institut für Mathematik, Martin-Luther-Universität Halle-Wittenberg, 06099 Halle (Saale), Germany

bending energy, i.e., (half of) the total squared curvature. The latter has a long history, dating back to Bernoulli, and can be seen as the starting point of elasticity theory.

The bending energy depends just on the centerline of an object and does not incorporate other physical effects such as twisting, friction, or shear. For instance, only relying on the bending energy one cannot explain why a telephone cable tends to curl. It also does not preclude self-penetration.

In this paper we extend the study of inextensible elastic curves by the first author [4] to inextensible and unshearable elastic rods. To this end we discretize the minimization problem

$$
\begin{cases}
\text{Minimize} \quad I_{\text{rod}}[y, b] = \dfrac{c_b}{2} \int_0^L |y''|^2 \, dx + \dfrac{c_t}{2} \int_0^L \big(b' \cdot (y' \times b)\big)^2 \, dx \\
\text{in the set } \mathcal{A} = \{(y, b) \in H^2 \times H^1 : L_{\text{bc}}^{\text{rod}}[y, b] = \ell_{\text{bc}}^{\text{rod}}, \\
\qquad\qquad\qquad |y'| = |b| = 1, \, y' \perp b\}.
\end{cases}
\tag{P_{rod}}
$$

and devise a numerical scheme in order to simulate a suitable H^2-like gradient flow.

Here c_b, $c_t > 0$ are bending and torsion rigidities that are determined by the Lamé coefficients of the material and geometrical properties of the rod. Furthermore, $L_{\text{bc}}^{\text{rod}} : H^2 \times H^1 \to Y$ encodes the boundary data $\ell_{\text{bc}}^{\text{rod}}$ in some finite-dimensional linear space Y. We assume that it only involves linear combinations of boundary points of y, y', and b. Therefore $L_{\text{bc}}^{\text{rod}}$ is continuous with respect to weak convergence in $H^2 \times H^1$. In particular $L_{\text{bc}}^{\text{rod}}$ can be used to incorporate periodicity in case of a closed curve y.

For ease of readability, we will rescale I_{rod} by $1/c_t$ from now on and abbreviate

$$
\varkappa = c_b/c_t.
$$

We will always assume $\mathcal{A}$ to be nonempty which is guaranteed if the boundary data $\ell_{\text{bc}}^{\text{rod}}$ is compatible with the frame condition and implies that the distance between the endpoints is strictly less than L. Any boundary data on a frame F can be matched by adjusting a reference frame F_0 using a suitable cumulative angle function φ (see Sect. 2.3 below).

Elastic rods

Based on the work of Mora and Müller [52] for general rods, the minimization problem (P_{rod}) can be rigorously derived from a general three-dimensional hyperelastic model, see [5] for a short formal derivation. In the situation of rods with circular cross-section, made of some isotropic and homogeneous material, we find that $c_b \geq 2c_t$. According to Coleman and Swigon [16, p. 195] there is some indication that values less than $\varkappa = \frac{3}{2}$ are appropriate for modeling DNA.

The study of elastic rods has a long history. It is closely related to elasticae, i.e., stationary points of the bending energy, see Levien [43] and references therein. A comprehensive presentation on the subject from the perspective of elasticity theory is provided by Antman [1].

We find applications in different fields such as the modeling of coiling and kinking of submarine cables (Zajac [76]; Goyal et al. [32,33]), cell filaments (Manhart et al. [46]), computer graphics (Bergou et al. [8]; Spillmann and Teschner [65]), and biomechanics [58]. Modeling in molecular biology and engineering has stimulated a lot of activity in this field as well.

A prototypical model for DNA supercoiling which has received considerable attention is the *twisted elastic ring* investigated by Maddocks in various collaborations [23,38,45,47,48]. The solution of the corresponding minimization problem leads to an intrinsically straight uniform rod with equal bending stiffness. The analysis bases on Hamiltonian formulations of rod mechanics. The general idea is to impose a twist rate β on a unit loop.

For small values of β the round circle (with a uniform twist) remains an equilibrium. This phenomenon is known as *Michell's instability* [50], see Goriely [29] and references therein. Larger perturbations lead to instability and bifurcation phenomena, cf. Goriely and Tabor [30,31].

Ivey and Singer [37] reconsidered the problem from a variational point of view, obtaining a complete description of the space of closed and quasiperiodic minimizers. Recently, a reformulation in terms of symplectic geometry has been given by Needham [53]. Regarding the discretization of elasticae we refer to Scholtes et al. [63].

Discretization

We aim at numerically detecting configurations of framed curves with low bending and twisting energy. For this we consider the gradient flow of the energy functional in (P$_{\text{rod}}$), a weighted sum of an elastic bending energy term and a functional that tracks the twisting of the frame about its centerline.

We implement a constraint ensuring that the curves stay close to arclength parametrization if the initial curve is arclength parametrized. Moreover the bending energy can be replaced by the squared L^2 norm of the second derivative of the curve which is a crucial point in the analysis of the discretization.

Related discretization approaches and the corresponding approximation results have been obtained by Le Tallec, Mani, and Rochinha [42] and Arunakirinathar and Reddy [2]. Here, we devise a discretization based on a reformulation of the energy functional that provides coercivity properties also when the frame constraints are only approximately satisfied. Moreover, the reformulation allows us to develop a fully practical and stable method for the iterative solution of the discrete variational problem.

The design of physically meaningful discretizations of rod models where twist is often modeled in terms of rotations is subject of continuing research in mechanical engineering. For instance, objective and path-independent interpolation strategies for so-called geometrically exact beams, including orthogonal (see, e.g., [62]) and non-orthogonal (see. e.g., [60]) interpolations of quaternions have been discussed. The situation becomes more involved on curved initial geometries [49]. An outline on major contributions to beam formulations can be found in [19].

Gradient flows

Recently, gradient flows involving the bending energy have received much attention, with respect to rigorous analysis, see Dziuk et al. [25], as well as regarding discretization aspects, see Deckelnick and Dziuk [22], Barrett et al. [3], Bartels [4], Dall'Acqua et al. [20], Pozzi and Stinner [57]. Lin and Schwetlick [44] also include frames in their model. A Newton scheme has been used in [42] to determine stationary configurations for the bending torsion model considered in this article.

Impermeability

Based on earlier work aiming at modeling DNA plasmids [15,18,71,73], Coleman and Swigon [16] take self-contact phenomena into account and discuss the interaction between certain topological quantities such as writhe, excess link, and the number of self-contact points. In [17] they include the case of (two-bridge) torus knots. In contrast to a related approach by Starostin [66] they impose a (small) positive thickness.

The corresponding case of open curves with appropriate boundary conditions has also been studied by several authors. Van der Heijden et al. [74] provide a comprehensive study of jump phenomena in clamped rods with and without self-contact. A more detailed classification of the respective equilibrium configurations is given by Neukirch and Henderson [54]. Clauvelin, Audoly, and Neukirch [14] modeled the situation of a small loosely knotted arc with open end-points and studied the shape of the set of self-contact and the influence of twist applied to the end-points as well. Starostin and van der Heijden [67] model the situation of so-called two-braids, i.e., structures formed by two elastic rods winding around each other, which also covers the case of $(2, b)$-torus knots [68,69]. The dynamic evolution of intertwined clamped loops subject to varying loads has been addressed by Goyal et al. [32,33].

Some of the above-mentioned models involve initial assumptions on the geometry, especially regarding the contact situation, focussing on explicit constructions for modeling and simulation. Our approach of treating (P_{rod}) does not rely on any precondition.

We will redefine (P_{rod}) in Sect. 6.6 to incorporate impermeability. To this end, we rely on the tangent-point energies whose impact on the evolution of (unframed) curves has been discussed in [6]. We thereby extend a regularization ansatz due to von der Mosel [75] with O'Hara's energies [55] in place of the tangent-point functional. In fact, one might conjecture that any self-avoiding functional will qualitatively produce the same results.

Computationally, this case is particularly challenging since strong forces related to bending effects have to by compensated by repulsive forces related to the tangent-point functional to avoid self-intersections. Regularization approaches guaranteeing global injectivity have been successfully implemented in different fields, see Krömer and Valdman [39] for an example in the context of elasticity.

The existence of curves minimizing (P_{rod}) follows via the direct method of the calculus of variations or, equally, from the Gamma-convergence (Proposition 1) together with the coercivity of the functionals. In the presence of uniform thickness bounds,

however, we cannot rely on these reasoning, see Gonzalez et al. [28]. While (P_{rod}) covers the "uniform symmetric case" of the Kirchhoff rod, which constitutes maybe the simplest model that involves both bending and twisting, the setting discussed in [28] offers more flexibility and especially also covers the cases of extensible shearable rods. Schuricht and von der Mosel [64] derived the Euler–Lagrange equations for elastic rods with self-contact. A similar approach has been followed by Hoffman and Seidman [34,35].

The evolution of impermeable rods preserves isotopy classes, so topology aspects come into play. Here we will encounter a more involved picture compared to the analysis of the twist-free setting, see Langer and Singer [40] and Gerlach et al. [26]. A complete characterization of minimizers is wide open.

Outline

We review the geometry of elastic rods in Sect. 2. In Sect. 3 we derive an approximation result (Lemma 1) that is used in Sect. 4 in order to prove Gamma-convergence of the discrete problem to the continuous one (Proposition 1). We prove stability of the numerical scheme in Sect. 5 (Proposition 2). Several experiments discussed in Sect. 6 indicate a complex energy landscape.

Notation

The inner products corresponding to L^2, H^1, H^2 are denoted by $(\cdot, \cdot)$, $(\cdot, \cdot)_{H^1}$, and $(\cdot, \cdot)_{H^2}$, respectively. The norms are written accordingly. Constants may change from line to line.

2 Elastic rods

Here we provide a short presentation of the geometry of elastic rods which is inspired by Langer, Singer and Ivey [37,41]. It is not essential for the analysis of the numerical scheme in the subsequent sections but sheds some light on the interpretation of the experiments in the last section.

2.1 Framed curves

A *rod* is modeled by a curve $y : [0, L] \to \mathbb{R}^3$ which corresponds to its centerline and an orthonormal *frame* $F : [0, L] \to SO(3)$ whose columns $F = [t, b, d]$ are called *directors*. Of course, $d = t \times b$ where $\times$ denotes the vector cross product. In the following we consider $y \in H^2$ and $F \in H^1$.

We will assume that the first column of F coincides with the unit tangent $t(x) = y'(x)/|y'(x)|$, $x \in [0, L]$. The idea is that the directors b and d track the twisting of the material about the centerline.

The assumed energy regime for bending stiffness in (P_{rod}) imposes inextensibility as a physical property. Therefore we can prescribe arclength parametrization which leads to the unit tangent vector $t = y'$ and the curvature $k = |t'| = |y''|$.

Our analysis also covers the case of closed rods where $[0, L]$ is understood to be the periodic interval $\mathbb{R}/L\mathbb{Z}$. We will realize the latter by imposing suitable (periodic) boundary conditions at 0 and L. In general a twist-free frame (see Sect. 2.3 below) of a closed curve will not close up, i.e., there can be a discontinuity at one point of $\mathbb{R}/L\mathbb{Z}$. One has to take care of this fact when defining boundary conditions.

An important frame that will always be well-defined and continuous for sufficiently smooth (both open and closed) curves y with nonvanishing curvature is the *Frénet frame* where $b_F = t'/|t'|$.

A rod is assumed to have some small diameter which can be considered infinitesimal; however, self-penetrations are not excluded at this stage (see Sect. 6.6 below for a discussion on modeling impermeability).

2.2 Twist rate

Using the orthonormality of the frame, we may express the variation of the director b by

$$b' = (b' \cdot t)t + (b' \cdot b)b + (b' \cdot d)d = -(b \cdot y'')t + (b' \cdot d)d.$$

The first term tracks the change of b that is imposed by the spatial behavior of the curve. It is just a component of the curvature vector as $y'' = (y'' \cdot b)b + (y'' \cdot d)d$. Only the second one actually provides information about the twisting of the frame about the centerline. Therefore we will call $b' \cdot d$ the *twist rate* of the frame.

We may also characterize a frame by a 9×9 linear system, namely

$$\begin{pmatrix} t \\ b \\ d \end{pmatrix}' = \begin{pmatrix} \mathbb{0} & k_b\mathbb{1} & k_d\mathbb{1} \\ -k_b\mathbb{1} & \mathbb{0} & \beta\mathbb{1} \\ -k_d\mathbb{1} & \beta\mathbb{1} & \mathbb{0} \end{pmatrix} \begin{pmatrix} t \\ b \\ d \end{pmatrix}$$

for scalar coefficient functions k_b, k_d, and β where $\mathbb{0}, \mathbb{1} \in \mathbb{R}^{3\times3}$ denote the zero and identity matrices. Here $k_b = y'' \cdot b$ and $k_d = y'' \cdot d$ are the components of the curvature k of y and $\beta = b' \cdot d$ is the twist rate. For instance, the Frénet frame is characterized by $k_d \equiv 0$.

A more detailed discussion of the impact of the twist rate is given in Sect. 2.4 below.

2.3 Reference frame

For any curve y, a point $\xi \in [0, L]$, and $\widehat{b} \in \mathbb{S}^2$, $\widehat{b} \perp y'(\xi)$, we obtain by integration a unique frame $F_0 = [t_0, b_0, d_0]$ for y with $F_0(\xi) = [y'(\xi), \widehat{b}, y'(\xi) \times \widehat{b}]$ whose twist rate is constantly zero. We call it synonymously a *Bishop frame*, *natural frame*, *reference frame*, or *twist-free* frame for y as it is a frame in rest position subject to a

fixed curve. Therefore, up to a rotation of the initial vector $\widehat{b}$ (which corresponds to an element of $\mathbb{S}^1$) there is a unique twist-free frame for any given curve.

A twist-free frame F_0 provides a useful reference configuration. Denoting the (cumulative) angle between the director b of any other frame and b_0 by φ, we arrive at $b = (\cos\varphi)b_0 + (\sin\varphi)d_0$ and $d = -(\sin\varphi)b_0 + (\cos\varphi)d_0$. Consequently, the rate of change of φ is just the twist rate

$$\varphi' = b' \cdot d = \beta. \tag{1}$$

Two frames that just differ by a constant angle φ may be considered equivalent, in particular when modeling rods with a circular diameter where there is no natural choice of a director. This is of course different for small ribbons with lateral extension in a particular direction.

Note that even for closed curves with frames that close up, $\varphi(L) - \varphi(0)$ does not need to be an integer multiple of 2π, unless the twist-free reference frame closes up. The latter applies in particular to rods with planar centerline where the vector being perpendicular to the respective plane provides a "canonical" twist-free frame.

In general, there is no direct correlation between $\varphi(L) - \varphi(0)$ and the angle enclosed by $b(0)$ and $b(L)$. One can think of a revolute joint that controls the latter angle.

2.4 Total twist

An important quantity, in the literature often simply referred to as "twist", is the *total twist* (more precisely, total twist rate)

$$\begin{aligned}
\mathrm{Tw}(y, b) &= \frac{\varphi(L) - \varphi(0)}{2\pi} = \frac{1}{2\pi} \int_0^L \varphi'(s)\,\mathrm{d}s = \frac{1}{2\pi} \int_0^L \beta(s)\,\mathrm{d}s \\
&= \frac{1}{2\pi} \int_0^L b'(s) \cdot d(s)\,\mathrm{d}s = \frac{1}{2\pi} \int_0^L \det\left(y'(s), b(s), b'(s)\right)\,\mathrm{d}s
\end{aligned}$$

where s is an arclength parameter and the last expression is parametrization invariant.

As the first identity suggests, the total twist can be interpreted as the number of rotations the director b (or, equivalently, d) performs about the curve, i.e., the centerline of the rod.

The total twist takes *integer* values on any closed curve for which both frame and twist-free reference frame close up (i.e., there are no discontinuities of the frames as periodic functions on $\mathbb{R}/L\mathbb{Z}$). In particular, this holds for any *planar* closed curve with a closed frame. In the latter case we can even compute the total twist by counting signed crossings of the corresponding link as follows.

A given (sufficiently smooth) embedded closed curve y together with a closed frame $[y', b, y' \times b]$ defines a *link* consisting of y and $y + \varepsilon b$ for some small $\varepsilon > 0$. Its Gauss linking number amounts to half of the sum of all signed crossings of y and $y + \varepsilon b$ with respect to a (regular) projection direction.

For embedded closed curves, the Gauss linking number decomposes into the sum of the total twist and the writhe functional. This identity has been derived by Călugăreanu [12,13]; see Moffatt and Ricca [51] for an account on the history of this result.

Writhe vanishes on planar (and spherical) embedded curves. Consequently, the total twist will be close to the Gauss linking number for embedded curves that are nearly planar. This applies to several situations in Sect. 6.

2.5 Energies

We assume that the behavior of the rod is driven by a linear combination of the *bending energy* (half of the total squared curvature) and the *twisting energy* (half of the total squared twist rate), cf. Mora and Müller [52]. More precisely we consider the functional

$$(y, b) \mapsto \frac{c_b}{2} \int_0^L k(s)^2 \, ds + \frac{c_t}{2} \int_0^L \beta(s)^2 \, ds \tag{2}$$

where s is an arclength parameter, $k(s)$ denotes the curvature of y at $y(s)$, and $c_b, c_t > 0$ are material constants. Minimizers are called *elastic rods*.

As mentioned in the introduction, we rescale the energy functional by $1/c_t$ and define $\varkappa = c_b/c_t$.

At the end of this section, we will briefly discuss two related minimization issues.

2.6 Optimal frames

For a given curve y, we may consider the problem to find a director b minimizing $I_{\text{rod}}[y, \cdot]$ subject to the boundary condition $L_{\text{bc}}^{\text{rod}}[y, b] = \ell_{\text{bc}}^{\text{rod}}$.

In first place, if b is a stationary point of $I_{\text{rod}}[y, \cdot]$ for some fixed y then

$$\beta \equiv \varphi' \equiv \frac{2\pi}{L} \text{Tw}(y, b) \tag{3}$$

is constant due to du Bois-Reymond's lemma. According to the Cauchy–Schwarz inequality, the twisting energy is bounded below by $\frac{2\pi^2}{L} \text{Tw}(y, b)^2$. This minimum is attained if and only if (3) holds such that the twisting energy then amounts to $\frac{2\pi^2}{L} \text{Tw}(y, b)^2 = \frac{L}{2} \beta^2$. In particular, we can check whether a given rod has a uniform twist rate by computing the quotient of total squared twist rate over squared total twist rate.

Note that for any global minimizer (y, b) of I_{rod}, the director b is a global minimizer of $I_{\text{rod}}[y, \cdot]$ as well.

In case $L_{\text{bc}}^{\text{rod}}[y, b]$ does not impose a condition on b at both points 0 and L, minimizing $I_{\text{rod}}[y, \cdot]$ is equivalent to constructing a twist-free frame.

Otherwise we face a *clamped problem*, i.e., b has to satisfy $b(0) = \widehat{b}_-$ and $b(L) = \widehat{b}_+$ for $\widehat{b}_-, \widehat{b}_+ \in \mathbb{S}^2$, $\widehat{b}_- \perp y'(0)$, $\widehat{b}_+ \perp y'(L)$. (If the boundary condition just forces the frame to close up, i.e., $b(0) = b(L)$, we may just let $\widehat{b}_- = \widehat{b}_+$ for an arbitrary vector perpendicular to $y'(0)$ and $y'(L)$.) In this case there is a global minimizer

$b_{\min}$ with constant twist rate (3). Using a twist-free reference frame $F_0 = [y', b_0, d_0]$ with $b_0 = \widehat{b}_-$ we have $\varphi(0) = 0$ and $\varphi(L) \in (-\pi, \pi]$. If $\varphi(L) \neq \pi$ there is a unique minimizer b with twist rate $\varphi' \equiv \frac{\varphi(L)}{L}$. If $\varphi(L) = \pi$ there are precisely two minimizers with twist rate $\varphi' \equiv \pm\frac{\pi}{L}$.

Topological restrictions can enforce arbitrary angles $\varphi(L) \in \mathbb{R}$, however, this does not apply to (P_{rod}) which does not preserve this sort of condition throughout the evolution. Keeping track of topology enforces modeling impermeability—quite a natural feature which we will address in Sect. 6.6.

2.7 Releasing total twist

In light of Sect. 2.6 we must have $|\text{Tw}(y, b)| \leq \frac{1}{2}$ for any global minimizer (y, b) of I_{rod}. In general, we have

$$|\text{Tw}(y, b)|^2 \leq \frac{L}{2\pi^2} \cdot \frac{1}{2} \int_0^L (b'(s) \cdot d(s))^2 \, ds,$$

however, the absolute value of the total twist does not have to be decreasing throughout the evolution.

At the final stage of an evolution of a closed curve (the frame does not have to close up), all we can hope for, however, is $|\text{Tw}(y, b)| \leq 1$. We briefly explain how this bound can be realized.

One can change the Gauss linking number of a given (embedded) rod by ± 2 by locally forming a small loop, performing a suitable self-penetration and moving the curve back to the original position. The value of the writhe functional is not affected as it only depends on the curve, not on the frame. So we have changed the total twist by ± 2 as well according to the Călugăreanu identity (cf. Sect. 2.4).

A self-penetration of the curve will in general lead to a change in topology resulting in a discontinuity of the linking number. While the total twist is continuous throughout the evolution, the writhe functional is not well-defined on non-embedded curves and thereby compensates the change of the linking number.

An evolution does not necessarily realize the bound $|\text{Tw}| \leq 1$. First of all, it is in general unclear whether it will in fact converge to a (local) minimizer at all. Another obstruction is discussed in the next section.

2.8 Michell's instability

Among all closed curves, the round circle framed by its Frénet normal vector is the unique global minimizer of I_{rod} (up to a constant rotation of the frame).

It is a remarkable fact that the round circle remains a minimizer (at least a local one, cf. Sect. 2.7) when we add some twist by increasing the (constant) twist rate β (which results in a discontinuity of the frame at one point). This phenomenon which is referred to as *Michell's instability* has been discovered 130 years ago [50] and then been rediscovered several times, see Goriely [29] for more details.

Zajac [76] has found the threshold $\beta_* = 2\pi\sqrt{3}\varkappa/L$ that separates the stable and unstable regime. As before, L denotes the length of the curve. More precisely, the circular rod is stable as long as $|\beta| < \beta_*$ and unstable if $|\beta| > \beta_*$. The dependency on $\varkappa = c_{\mathrm{b}}/c_{\mathrm{t}}$ is quite intuitive: If $\varkappa$ is very big, the bending energy dominates which always prefers the circle. A proof of Zajac's result adapted to our setting can be found in Ivey and Singer [37, Sect. 6].

Values of $\varkappa < \frac{1}{3}\sqrt{3} \approx 0.5774$ lead to an initial twist $\beta_* < \frac{2\pi}{L}$. Starting an evolution with $\beta_{\mathrm{ini}} \in \left(\beta_*, \frac{2\pi}{L}\right)$, we have $|\mathrm{Tw}| = \mathrm{Tw} < 1$. Therefore the rod cannot reduce twist by self-penetration, so we will merely face some buckling of the rod—which is difficult to detect numerically. In Experiment 6.2 we chose $\varkappa = \frac{3}{2}$, for which we measure a drastic change of the twisting energy by self-penetration of the curve.

Interestingly, Michell's instability does not occur for initially curved curves, see Olsen et al. [72] and Hu [36].

3 Density

We can smoothly approximate any framed curve in $\mathcal{A}$, i.e., $\mathcal{A} \cap (C^\infty \times C^\infty)$ is dense in $\mathcal{A}$ with respect to the $H^2 \times H^1$-topology, preserving given boundary conditions.

Lemma 1 *For any rod $(y, b) \in \mathcal{A}$ and $\varepsilon > 0$ there is another rod $(y_\varepsilon, b_\varepsilon) \in \mathcal{A} \cap (C^\infty \times C^\infty)$ with $\|y_\varepsilon - y\|_{H^2} \leq \varepsilon$ and $\|b_\varepsilon - b\|_{H^1} \leq \varepsilon$.*

Proof Our strategy is as follows. We first construct smooth approximizers $(y_\delta, b_\delta) \in C^\infty \times C^\infty$. In a second step we correct the boundary values by adding (smooth) functions v_δ and c_δ. The new curve $y_\delta + v_\delta$ will not have length L. We balance the length by adding another smooth function w_δ compactly supported in $(0, L) \backslash \mathrm{supp}\, v_\delta$. Now we reparametrize the curve $y_\delta + v_\delta + w_\delta$ to arclength and apply the same reparametrization to the vector field $b_\delta + c_\delta$. Renormalizing it by the usual Gram–Schmidt scheme produces the required director.

We choose $\delta \in (0, \delta_0]$ for some $\delta_0 \in (0, 1]$ which will be fixed later on only depending on (y, b) and ε. Using a standard mollifier, we obtain $(y_\delta, b_\delta) \in C^\infty((0, L), \mathbb{R}^3) \times C^\infty((0, L), \mathbb{R}^3)$ with $\|y_\delta - y\|_{H^2} \leq \delta$ and $\|b_\delta - b\|_{H^1} \leq \delta$.

In order to match the boundary conditions, we subtract suitable functions. More precisely, we let

$$\begin{aligned}
\bar{y}_\delta = y_\delta + v_\delta &= y_\delta - (y_\delta(0) - y(0))\zeta_0 - (y'_\delta(0) - y'(0))\zeta_1 \\
&\quad - (y_\delta(L) - y(L))\zeta_0(L - \cdot) + (y'_\delta(L) - y'(L))\zeta_1(L - \cdot), \\
\bar{b}_\delta = b_\delta + c_\delta &= b_\delta - (b_\delta(0) - b(0))\zeta_0 - (b_\delta(L) - b(L))\zeta_0(L - \cdot)
\end{aligned}$$

where $\zeta_0, \zeta_1 \in C^\infty([0, L])$ fulfill $\zeta_j(0) = \delta_{j,0}$, $\zeta'_j(0) = \delta_{j,1}$, $\zeta_j|_{[\mu, L]} \equiv 0$, $j = 0, 1$, for some $\mu \in (0, L/2)$ to be determined later.

By construction we have $L^{\mathrm{rod}}_{\mathrm{bc}}[\bar{y}_\delta, \bar{b}_\delta] = L^{\mathrm{rod}}_{\mathrm{bc}}[y, b] = \ell^{\mathrm{rod}}_{\mathrm{bc}}$ as well as

$$\|\bar{y}_\delta - y_\delta\|_{H^2} \leq C_\mu \|y_\delta - y\|_{C^1} \leq C_\mu \widetilde{C} \delta,$$

$$\left\| \bar{b}_\delta - b_\delta \right\|_{H^1} \le C_\mu \left\| b_\delta - b \right\|_{C^0} \le C_\mu \tilde{C} \delta$$

where C_μ only depends on μ and $\tilde{C} > 0$ on the embedding $H^1 \hookrightarrow C^0$.

Now we prepare the length correction. If $|y(L) - y(0)| = L$, the curve y just parametrizes the segment from $y(0)$ to $y(L)$, so $y \in C^\infty$ and we only have to treat the director b (which can be done similarly as outlined below). If $|y(L) - y(0)| < L$ we infer from $H^2 \subset C^1$ that $y \in \mathcal{A}$ cannot only move on a straight line. So we may assume that there is some constant unit vector $\mathbf{v} \in \mathbb{S}^2$, $\mathbf{v} \perp (y(L) - y(0))$ (this condition is empty for closed curves), such that $y' \cdot \mathbf{v} > 0$ on some closed interval $I_+ \subset [0, L]$. Due to the fact that $\int_0^L y'(x) \cdot \mathbf{v} \, dx = (y(L) - y(0)) \cdot \mathbf{v} = 0$ there has to be another closed interval $I_- \subset [0, L]$ on which $y' \cdot \mathbf{v} < 0$. Diminishing $I_\pm$ if necessary, they have positive distance to the boundary points 0 and L. Now we may choose $\mu \in (0, L/2)$ such that they are both contained in $(\mu, L - \mu)$.

As the intervals are closed there is some $\lambda \in (0, \frac{1}{2}]$ such that $\pm y' \cdot \mathbf{v} \ge 2\lambda$ on $I_\pm$. Diminishing δ_0 if necessary, we may assume that $\pm y_\delta' \cdot \mathbf{v} \ge \lambda$ on $I_\pm$ for all $\delta \in (0, \delta_0]$.

The length correction function will be defined by $w_\delta = \omega_\delta \phi \mathbf{v}$ for some $\omega_\delta \in \mathbb{R}$ to be defined later and $\phi \in C^\infty([0, L])$ is compactly supported in $(0, L)$ with $\pm \phi' \ge 0$ on $I_\pm$ and $\phi' \equiv 0$ elsewhere, but $\phi \not\equiv 0$.

The idea is that by choosing ω_δ accordingly, we can correct the length of (y_δ and) $\bar{y}_\delta$ by an amount between $[-\alpha, \alpha]$ where $\alpha > 0$ does not depend on δ (nor δ_0). As $\mathcal{L}[\bar{y}_\delta] \to L$ for $\delta \searrow 0$ we can perform the length correction if δ_0 is small enough. Furthermore, $\omega_\delta \to 0$ as $\delta \searrow 0$.

To make this more precise, let $w = \omega \phi \mathbf{v}$ for some $\omega \in \mathbb{R}$ with

$$|\omega| \le \frac{\lambda}{\|\phi'\|_{C^0}}.$$

As $y_\delta' \cdot \mathbf{v} \phi'$ is bounded below by $\lambda |\phi'|$ on $[0, L]$, we obtain

$$
\frac{\left| y_\delta' + w' \right|^2 - \left| y_\delta' \right|^2}{\omega} = 2 y_\delta' \cdot \mathbf{v} \phi' + \omega \phi'^2 \ge 2\lambda |\phi'| - |\omega| \phi'^2 \ge \lambda |\phi'|,
$$
$$
\left| y_\delta' + w' \right| + \left| y_\delta' \right| \le 2 \left| y_\delta' \right| + \left| w' \right| \le 2 \left(1 + \left| y_\delta' - y' \right| \right) + |\omega| \left| \phi' \right|
$$
$$
\le 2 \left(1 + \tilde{C} \delta_0 \right) + \lambda \le 2 \left(2 + \tilde{C} \right),
$$
$$
\frac{\left| y_\delta' + w' \right| - \left| y_\delta' \right|}{\omega} \ge \frac{\left| y_\delta' + w' \right|^2 - \left| y_\delta' \right|^2}{\omega \left(\left| y_\delta' + w' \right| + \left| y_\delta' \right| \right)} \ge \frac{\lambda |\phi'|}{2 \left(2 + \tilde{C} \right)}.
$$

Therefore,

$$
\left| y_\delta' + w' \right| \begin{cases} \le \left| y_\delta' \right| - |\omega| \frac{\lambda |\phi'|}{2(2+\tilde{C})} & \text{if } \omega \le 0, \\ \ge \left| y_\delta' \right| + |\omega| \frac{\lambda |\phi'|}{2(2+\tilde{C})} & \text{if } \omega \ge 0. \end{cases}
$$

Recalling that v_δ and w have disjoint support, we infer

$$\left| y'_\delta + v'_\delta + w' \right| \begin{cases} \le \left| y'_\delta + v'_\delta \right| - |\omega| \frac{\lambda |\phi'|}{2(2+\widetilde{C})} & \text{if } \omega \le 0, \\ \ge \left| y'_\delta + v'_\delta \right| + |\omega| \frac{\lambda |\phi'|}{2(2+\widetilde{C})} & \text{if } \omega \ge 0, \end{cases}$$

which allows for the desired length correction depending on the sign of ω. More precisely, we can change the length of $y_\delta + v_\delta$ by at least $\pm \alpha$ where $\alpha = \frac{\lambda^2 \|\phi'\|_{L^1}}{2(2+\widetilde{C})\|\phi'\|_{C^0}}$. Diminishing δ_0 if necessary, we can ensure that $|\mathcal{L}(y_\delta + v_\delta) - L| \le \alpha$. So we can find $\omega = \omega_\delta$ such that the curve $\bar{\bar{y}}_\delta = y_\delta + v_\delta + w_\delta$ has length L with $L_{\mathrm{bc}}^{\mathrm{rod}}[\bar{\bar{y}}_\delta, \bar{b}_\delta] = \ell_{\mathrm{bc}}^{\mathrm{rod}}$.

The embedding $H^1 \hookrightarrow C^0$ guarantees that the curve $\bar{\bar{y}}_\delta$ is immersed and $\min \left| \bar{b}_\delta \right| \ge \frac{1}{2}$ if δ_0 is small enough. So we may apply the reparametrization operator from Lemma 2 and let $\breve{y}_\delta = \bar{\bar{y}}_\delta \circ \psi_{\bar{\bar{y}}_\delta}^{-1}$ and $\breve{b}_\delta = \bar{b}_\delta \circ \psi_{\bar{\bar{y}}_\delta}^{-1}$. We still have $\min \left| \breve{b}_\delta \right| \ge \frac{1}{2}$. Now

$$\left\| \bar{\bar{y}}_\delta - y \right\|_{H^2} \le \|y_\delta - y\|_{H^2} + \|v_\delta\|_{H^2} + \|w_\delta\|_{H^2} \le \delta + C_\mu \widetilde{C}\delta + \omega_\delta \|\phi\|_{H^2}$$

and $\left\| \bar{b}_\delta - b \right\|_{H^1}$ tend to zero as $\delta \searrow 0$. Using the continuity of the reparametrization and $|y'| \equiv 1$ we find that $\left\| \breve{y}_\delta - y \right\|_{H^2}$ tends to zero as well. Choosing δ_0 sufficiently small, we may assume that $\left\| \breve{y}_\delta - y \right\|_{H^2} \le \varepsilon$ and $\left\| \bar{b}_\delta - b \right\|_{H^1} \le \frac{\varepsilon}{4}$, and additionally $\left\| \breve{b}_\delta - \bar{b}_\delta \right\|_{H^1} \le \frac{\varepsilon}{4}$ since $\psi_{\bar{\bar{y}}_\delta} \to \mathrm{id}_{[0,L]}$ with respect to H^2-convergence. Note that $(\breve{y}_\delta, \breve{b}_\delta)$ are still C^∞-smooth with $L_{\mathrm{bc}}^{\mathrm{rod}}[\breve{y}_\delta, \breve{b}_\delta] = \ell_{\mathrm{bc}}^{\mathrm{rod}}$.

It remains to correct the director. To this end, we let $\widetilde{b}_\delta = \breve{b}_\delta - \left(\breve{b}_\delta \cdot \breve{y}'_\delta \right) \breve{y}'_\delta$. We have $\left\| \widetilde{b}_\delta - \breve{b}_\delta \right\|_{H^1} \le \frac{\varepsilon}{4}$ and $\left\| \widetilde{b}_\delta / |\widetilde{b}_\delta| - \widetilde{b}_\delta \right\|_{H^1} \le \frac{\varepsilon}{4}$ if δ_0 is sufficiently small. Indeed, using Leibniz rule $\|vw\|_{H^1} \le \|v\|_{H^1} \|w\|_{H^1}$ and the fact that both $\left\| \breve{y}_\delta - y \right\|_{H^2}$ and $\left\| \breve{b}_\delta - b \right\|_{H^1}$ get arbitrarily small provided δ_0 is chosen accordingly, the same applies to

$$\left\| \widetilde{b}_\delta - \breve{b}_\delta \right\|_{H^1} = \left\| \left(\breve{b}_\delta \cdot \breve{y}'_\delta \right) \breve{y}'_\delta \right\|_{H^1} = \left\| \left(\breve{b}_\delta \cdot \breve{y}'_\delta - b \cdot y' \right) \breve{y}'_\delta \right\|_{H^1}$$

$$\le \left(\left\| \breve{b}_\delta - b \right\|_{H^1} \left\| \breve{y}'_\delta \right\|_{H^1} + \|b\|_{H^1} \left\| \breve{y}'_\delta - y' \right\|_{H^1} \right) \left\| \breve{y}'_\delta \right\|_{H^1}$$

$$\le \left(\left\| \breve{b}_\delta - b \right\|_{H^1} \left(\|y'\|_{H^1} + \varepsilon \right) + \|b\|_{H^1} \left\| \breve{y}'_\delta - y' \right\|_{H^1} \right) \left(\|y'\|_{H^1} + \varepsilon \right),$$

and

$$\left\| \frac{\widetilde{b}_\delta}{|\widetilde{b}_\delta|} - \widetilde{b}_\delta \right\|_{H^1} = \left\| \widetilde{b}_\delta \cdot \frac{1 - |\widetilde{b}_\delta|}{|\widetilde{b}_\delta|} \right\|_{H^1} \le \left\| \widetilde{b}_\delta \right\|_{H^1} \left\| \frac{|b| - |\widetilde{b}_\delta|}{|\widetilde{b}_\delta|} \right\|_{H^1}$$

$$\le \left(\|b\|_{H^1} + \varepsilon \right) \left\| \frac{\langle \widetilde{b}_\delta + b, \widetilde{b}_\delta - b \rangle}{|\widetilde{b}_\delta| + |b|} \right\|_{H^1} \left\| \frac{1}{|\widetilde{b}_\delta|} \right\|_{H^1}$$

$$\le \left(2\left\|b\right\|_{H^1} + \varepsilon\right)^2 \left\|\frac{1}{\left|\widetilde{b}_\delta\right| + |b|}\right\|_{H^1} \left\|\frac{1}{\left|\widetilde{b}_\delta\right|}\right\|_{H^1} \left\|\widetilde{b}_\delta - b\right\|_{H^1}.$$

Arguing as above, we find that the term $\left\| 1/\left|\widetilde{b}_\delta\right| \right\|_{H^1}$ is uniformly bounded. In fact, from $\left|\widetilde{b}_\delta \cdot \widetilde{y}_\delta'\right| = \left|\widecheck{b}_\delta \cdot \widecheck{y}_\delta' - b \cdot y'\right| \xrightarrow{\delta \searrow 0} 0$ we infer $\left|\widetilde{b}_\delta\right| \ge \frac{1}{4}$ if δ_0 is sufficiently small. This allows for bounding $\left\| \left(1/\left|\widetilde{b}_\delta\right|\right)'\right\|$ as well. In the same way we prove boundedness of $\left\| 1/\left(\left|\widetilde{b}_\delta\right| + |b|\right)\right\|_{H^1}$. Letting $(y_\varepsilon, b_\varepsilon) = \left(\widecheck{y}_{\delta_0}, \widetilde{b}_{\delta_0}/\left|\widetilde{b}_{\delta_0}\right|\right) \in \mathcal{A} \cap (C^\infty \times C^\infty)$ finishes the proof. □

Let $H_r^2((0, L), \mathbb{R}^3)$ denote the (open) subset of regular (i.e., non-vanishing derivative) curves in $H^2((0, L), \mathbb{R}^3)$.

Lemma 2 *The operator $H_r^2((0, L), \mathbb{R}^3) \to H_r^2((0, L), \mathbb{R}^3)$ defined by*

$$y \mapsto y \circ \psi_y^{-1} \quad \text{where} \quad \psi_y(x) = \frac{L}{\mathscr{L}[y]}\mathscr{L}\left[y|_{[0,x]}\right]$$

that reparametrizes an immersed curve to constant speed is continuous with respect to the H^2-norm. Moreover, $y \circ \psi_y^{-1} \in C^\infty$ if $y \in C^\infty$ is immersed.

A proof can be found in [59, Appendix]; the argument applies without rescaling and the additional requirement of embeddedness. It applies to non-periodic intervals $[0, L]$ as well. The last statement can be derived from the formula.

4 Discretization

Our discretization is based on cubic and linear finite element spaces. We consider a partition of $[0, L]$ by a set of nodes $\mathcal{N}_h$ that contains the endpoints 0 and L. We define nodal bases $(\varphi_z)_{z \in \mathcal{N}_h}$ and $(\psi_{z,j})_{z \in \mathcal{N}_h}$, $j = 0, 1$ with the following properties. If $z_\pm \in \mathcal{N}_h$ are neighboring nodes of $z \in \mathcal{N}_h$ then φ_z and $\psi_{z,j}$ are supported in $[z_-, z_+]$. On the intervals $[z_-, z]$ and $[z, z_+]$ the functions φ_z are (affine) linear with $\varphi_z(z) = 1$ while $\psi_{z,j}$ are cubic polynomials satisfying $\psi_{z,j}(z) = \delta_{j,0}$ and $\psi_{z,j}'(z) = \delta_{j,1}$, $j = 0, 1$. We define nodal interpolation operators on $C^0([0, L])$ and $C^1([0, L])$ respectively by letting

$$\mathcal{I}_h^{1,0} v = \sum_{z \in \mathcal{N}_h} v(z)\varphi_z,$$

$$\mathcal{I}_h^{3,1} w = \sum_{z \in \mathcal{N}_h} \left(w(z)\psi_{z,0} + w'(z)\psi_{z,1}\right).$$

Furthermore, we will employ the averaging operator Q_h which is piecewise defined on any element $[z, z']$ (i.e., $z, z' \in \mathcal{N}_h$ are neighboring) by

$$Q_h v(x) = \frac{1}{z' - z} \int_z^{z'} v(\xi) \, d\xi, \qquad x \in (z, z').$$

We have $\|v - Q_h v\|_{L^\infty} \leq Ch^\alpha [v]_{C^{0,\alpha}}$ for all $v \in C^{0,\alpha}$, $\alpha \in (0, 1]$ and $\|Q_h v_h\|_{L^\infty} \leq \|v_h\|_{L^\infty}$ for all piecewise linear functions v_h subject to $\mathcal{N}_h$.

Both for the discrete approximation result and the stability of our numerical scheme presented in Sect. 5 below it is crucial to exploit the structure of the dimensionally reduced functionals.

To identify convex and concave terms, we observe that the orthonormality of the frame $F = [t, b, d]$ implies $b' \cdot b = 0$ and $b' \cdot t = -b \cdot t'$. Therefore the integrand of the twisting functional becomes $(b' \cdot d)^2 = |b'|^2 - (b \cdot t')^2$.

To obtain a coercivity property (under the restriction $\|b_h\|_{L^\infty} \leq 1$) we set

$$\theta = \min\left\{\frac{\varkappa}{2}, 1\right\} \quad \in (0, 1] \tag{4}$$

which ensures $\varkappa \geq 2\theta$. This will allow for controlling (part of) the second term of $I_{\text{rod}}[y, b]$ by the first one even if $\varkappa < 2$. Now we decompose

$$
\begin{aligned}
I_{\text{rod}}[y, b] &= \frac{\varkappa}{2} \int_0^L |y''|^2 \, dx + \frac{1}{2} \int_0^L (b' \cdot d)^2 \, dx \\
&= \frac{\varkappa}{2} \int_0^L |y''|^2 \, dx + \frac{\theta}{2} \int_0^L |b'|^2 \, dx - \frac{\theta}{2} \int_0^L (b \cdot y'')^2 \, dx \\
&\quad + \frac{1 - \theta}{2} \int_0^L (b' \cdot (y' \times b))^2 \, dx.
\end{aligned}
$$

By $V_{\text{rod}}^h \subset H^2 \times H^1$ we denote the cross product of piecewise cubic and piecewise linear functions subject to $\mathcal{N}_h$. With the product finite element space V_{rod}^h and the operator Q_h we consider the following discretization of the minimization problem (P_{rod}) in which the pointwise orthogonality relation $y' \cdot b = 0$ is approximated via a penalty term. To this end we discretize the minimization problem

$$
\left\{
\begin{aligned}
&\text{Minimize} \quad I_{\text{rod}}^{h,\varepsilon}[y_h, b_h] = \frac{\varkappa}{2} \int_0^L |y_h''|^2 \, dx + \frac{\theta}{2} \int_0^L |b_h'|^2 \, dx \\
&\qquad - \frac{\theta}{2} \int_0^L (Q_h b_h \cdot y_h'')^2 \, dx + \frac{1}{2\varepsilon} \int_0^L \mathcal{I}_h^{1,0}[(y_h' \cdot b_h)^2] \, dx \\
&\qquad + \frac{1 - \theta}{2} \int_0^L (b_h' \cdot (y_h' \times Q_h b_h))^2 \, dx \\
&\text{in the set } \mathcal{A}_h = \{(y_h, b_h) \in V_{\text{rod}}^h : L_{\text{bc}}^{\text{rod}}[y_h, b_h] = \ell_{\text{bc}}^{\text{rod}}, \\
&\qquad\qquad |y_h'(z)| = |b_h(z)| = 1 \text{ f.a. } z \in \mathcal{N}_h\}.
\end{aligned}
\right. \quad (P_{\text{rod}}^{h,\varepsilon})
$$

The operators Q_h and $\mathcal{I}_h^{1,0}$ are included in a way that leads to a simple assembly of the corresponding matrices and avoids quadrature.

Note that the constraints are imposed on particular degrees of freedom which makes the method practical. In order to ensure $\mathcal{A}_h \neq \emptyset$, the distance between the endpoints of y_h must be less than L and the spatial mesh has to be chosen sufficiently fine.

For establishing the Gamma-convergence result, it is useful to write

$$I_{\text{rod}}[y, b] = \frac{\varkappa - \theta}{2} \left\| y'' \right\|^2 + \frac{\theta}{2} \left\| b' \right\|^2 + \frac{\theta}{2} \left\| P_b y'' \right\|^2 + \frac{1 - \theta}{2} \left\| b' \cdot (y' \times b) \right\|^2,$$

$$I_{\text{rod}}^{h,\varepsilon}[y_h, b_h] = \frac{\varkappa - \theta}{2} \left\| y_h'' \right\|^2 + \frac{\theta}{2} \left\| b_h' \right\|^2 + \frac{\theta}{2} \left\| P_{Q_h b_h} y_h'' \right\|^2$$

$$+ \frac{1 - \theta}{2} \left\| b_h' \cdot (y_h' \times Q_h b_h) \right\|^2 + \frac{1}{2\varepsilon} \int_0^L \mathcal{I}_h^{1,0}[(y_h' \cdot b_h)^2] \, dx$$

where P_b and $P_{Q_h b_h}$ denote the square roots of the positive semidefinite matrices $\mathbb{1} - b \otimes b$ and $\mathbb{1} - Q_h b_h \otimes Q_h b_h$ respectively.

The only difference to I_{rod} is the penalization term and the fact that b is replaced by $Q_h b_h$ in the third term and once in the fourth term.

Our first task is to show that minimizers of $I_{\text{rod}}^{h,\varepsilon}$ within $\mathcal{A}_h$ approximate I_{rod}-minimizers within $\mathcal{A}$. In the following statement, we assume that I_{rod} and $I_{\text{rod}}^{h,\varepsilon}$ attain the value $+\infty$ outside of $\mathcal{A}$ and $\mathcal{A}_h$, respectively.

Proposition 1 *As $\varepsilon, h \searrow 0$, the functional $I_{\text{rod}}^{h,\varepsilon}$ Gamma-converges to I_{rod} with respect to the weak $H^2 \times H^1$-topology.*

Note that there is no restriction on the ratio of ε and h.

Le Tallec et al. [42, Thm. 1] have derived a related result using different arguments. They show that any isolated minimum of the continuous problem is the strong limit of a sequence of local minima of the finite element problem. To approximate rods within finite element spaces, they consider interpolants and then correct the orthogonalities by an iterative scheme [42, Thm. 2]. Thereby they obtain admissible rods only in the limit. Although we could employ the latter result in the following proof, we prefer Lemma 1 which provides a constructive argument.

Proof To establish the *Lim-inf inequality*, we consider an arbitrary sequence $((y_h, b_h))_{h>0} \subset \mathcal{A}_h$ and $(y, b) \in H^2 \times H^1$ with $y_h \rightharpoonup y$ in H^2 and $b_h \rightharpoonup b$ in H^1 as $h \searrow 0$. In particular, we have $y_h \to y$ in C^1 and $b_h \to b$ in C^0.

We have to show that if $\liminf_{(h,\varepsilon) \searrow 0} I_{\text{rod}}^{h,\varepsilon}[y_h, b_h] < \infty$ then the limit point (y, b) belongs to $\mathcal{A}$ (such that the formula for I_{rod} is applicable) and the lim inf-inequality holds.

As the mesh size tends to zero as $h \searrow 0$, the condition $|y'| = |b| = 1$ is satisfied everywhere due to the uniform convergence $y_h' \to y'$, $b_h \to b$. Furthermore $L_{\text{bc}}^{\text{rod}}$ is continuous with respect to weak convergence. It remains to verify that b is perpendicular to y'. By the interpolation estimate we have

$$\left\| (y_h' \cdot b_h)^2 - \mathcal{I}_h^{1,0}\left[(y_h' \cdot b_h)^2 \right] \right\| \leq C h \left\| \left((y_h' \cdot b_h)^2 \right)' \right\|$$

$$\leq Ch \left\| y_h' \right\|_{L^\infty} \left\| b_h \right\|_{L^\infty} \left\| y_h' \right\|_{H^1} \left\| b_h \right\|_{H^1}.$$

As $y_h' \cdot b_h \to y' \cdot b$ in C^0, we infer

$$\int_0^L \mathcal{I}_h^{1,0} \left[(y_h' \cdot b_h)^2 \right] dx \to \int_0^L (y' \cdot b)^2 \, dx.$$

As all terms of $I_{\text{rod}}^{h,\varepsilon}$ are non-negative, the term $\varepsilon^{-1} \int_0^L \mathcal{I}_h^{1,0} \left[(y_h' \cdot b_h)^2 \right] dx$ is uniformly bounded which implies $\int_0^L (y' \cdot b)^2 \, dx = 0$. This gives $y' \perp b$, so $(y, b) \in \mathcal{A}$.

We use $\| Q_h b_h + b \|_{L^\infty} \leq 2$ to derive

$$\begin{aligned}
\left\| P_b y_h'' \right\|^2 &= \left\| P_{Q_h b_h} y_h'' \right\|^2 - \left\| b \cdot y_h'' \right\|^2 + \left\| Q_h b_h \cdot y_h'' \right\|^2 \\
&\leq \left\| P_{Q_h b_h} y_h'' \right\|^2 + 2 \left\| Q_h b_h - b \right\|_{L^\infty} \left\| y_h'' \right\|^2.
\end{aligned}$$

The second term on the right-hand side tends to zero as $h \searrow 0$ due to the boundedness of weakly converging sequences and

$$\| Q_h b_h - b \|_{L^\infty} \leq \| Q_h b_h - b_h \|_{L^\infty} + \| b_h - b \|_{L^\infty} \leq C\sqrt{h} + o(1). \tag{5}$$

This estimate also yields $y_h' \times Q_h b_h \to y' \times b$ in L^2 which implies $b_h' \cdot (y_h' \times Q_h b_h) \rightharpoonup b' \cdot (y' \times b)$ (weakly) in L^2 as $h \searrow 0$.

Now the lim inf-inequality follows from the lower semicontinuity of the L^2-norm and the fact that the penalization term is non-negative (since it is the linear interpolation of a non-negative term).

We turn to the *Lim-sup inequality*. Let $(y, b) \in \mathcal{A}$ and $\delta \in (0, 1]$. Of course, $I_{\text{rod}}[y, b] < \infty$. We aim at constructing a recovery sequence. We apply Lemma 1 to obtain $(\widetilde{y}_\delta, \widetilde{b}_\delta) \in \mathcal{A} \cap (C^\infty \times C^\infty)$ with $\| \widetilde{y}_\delta - y \|_{H^2} \leq \delta$ and $\| \widetilde{b}_\delta - b \|_{H^1} \leq \delta$. We let $(y_h, b_h) = \left(\mathcal{I}_h^{3,1} \widetilde{y}_\delta, \mathcal{I}_h^{1,0} \widetilde{b}_\delta \right)$. Owing to the smoothness of the regularized rod, we have $\| y_h - \widetilde{y}_\delta \|_{H^2} \leq C_\delta h$ and $\| b_h - \widetilde{b}_\delta \|_{H^1} \leq C_\delta h$. In particular, $(y_h, b_h) \in \mathcal{A}_h$. We have to bound $I_{\text{rod}}^{h,\varepsilon}[y_h, b_h] - I_{\text{rod}}[y, b]$ above by an expression that tends to zero. For the first three terms of $I_{\text{rod}}^{h,\varepsilon}[y_h, b_h]$, we obtain

$$\begin{aligned}
\left\| y_h'' \right\|^2 - \left\| y'' \right\|^2 &\leq \left\| y_h'' + y'' \right\| \left\| y_h'' - y'' \right\| \\
&\leq \left(2 \left\| y'' \right\| + \delta + C_\delta h \right) (\delta + C_\delta h), \\
\left\| b_h' \right\|^2 - \left\| b' \right\|^2 &\leq \left(2 \left\| b' \right\| + \delta + C_\delta h \right) (\delta + C_\delta h), \\
\left\| P_{Q_h b_h} y_h'' \right\|^2 - \left\| P_b y'' \right\|^2 &\leq \left\| y_h'' \right\|^2 - \left\| y'' \right\|^2 + \left\| b \cdot y'' \right\|^2 - \left\| Q_h b_h \cdot y_h'' \right\|^2.
\end{aligned}$$

For the last two terms in the previous line, we infer

$$\begin{aligned}
\left\| b \cdot y'' \right\|^2 - \left\| Q_h b_h \cdot y_h'' \right\|^2 &\leq \left\| Q_h b_h \cdot y_h'' + b \cdot y'' \right\| \left\| Q_h b_h \cdot y_h'' - b \cdot y'' \right\| \\
&\leq \left(2 \left\| b \cdot y'' \right\| + \left\| Q_h b_h \cdot y_h'' - b \cdot y'' \right\| \right) \left\| Q_h b_h \cdot y_h'' - b \cdot y'' \right\|
\end{aligned}$$

and, recalling (5),

$$\left\| Q_h b_h \cdot y_h'' - b \cdot y'' \right\| \le \left\| Q_h b_h - b \right\|_{L^\infty} \left\| y_h'' \right\| + \left\| y_h'' - y'' \right\|$$
$$\le \left(C\sqrt{h} + \delta + C_\delta h \right) \left(\left\| y'' \right\| + \delta + C_\delta h \right) + \delta + C_\delta h.$$

We treat the fourth term of $I_{\mathrm{rod}}^{h,\varepsilon}[y_h, b_h]$ similarly as above. More precisely, we infer

$$\left\| b_h' \cdot (y_h' \times Q_h b_h) \right\|^2 - \left\| b' \cdot (y' \times b) \right\|^2$$
$$= \left\| b_h' \cdot (y_h' \times Q_h b_h) + b' \cdot (y' \times b) \right\| \left\| b_h' \cdot (y_h' \times Q_h b_h) - b' \cdot (y' \times b) \right\|$$
$$\le \left(\left\| b_h' \right\| \left\| y_h' \right\|_{L^\infty} \left\| b_h \right\|_{L^\infty} + \left\| b' \right\| \right) \cdot$$
$$\quad \cdot \left(\left\| b_h' - b' \right\| \left\| y_h' \right\|_{L^\infty} \left\| b_h \right\|_{L^\infty} + \left\| b' \right\| \left\| y_h' - y' \right\|_{L^\infty} \left\| b_h \right\| + \left\| b' \right\| \left\| Q_h b_h - b \right\| \right).$$

Finally we deal with the penalty term. Due to $\widetilde{y_\delta}' \perp \widetilde{b_\delta}$ we find that $y_h'(z) \cdot b_h(z) = 0$ for all $z \in \mathcal{N}_h$. Therefore $\mathcal{I}_h^{1,0}\left[(y_h' \cdot b_h)^2 \right](x) = 0$ for all $x \in I$ which implies that the penalty term vanishes on the entire sequence. $\qquad\square$

5 Iterative minimization

We linearize the pointwise constraints in our iterative algorithm for computing minimizers of $I_{\mathrm{rod}}^{h,\varepsilon}$. Let $\mathcal{T}_h$ be a partition of $[0, L]$ with respect to the set of nodes $\mathcal{N}_h$. By $\mathcal{S}^{m,k}(\mathcal{T}_h)$ we denote the set of $C^k([0, L])$ functions whose restriction on any subinterval from $\mathcal{T}_h$ is a polynomial of degree at most m.

For a vector field $y_h \in \mathcal{S}^{3,1}(\mathcal{T}_h)^3$ we set

$$\mathcal{F}_h[y_h] = \{ w_h \in \mathcal{S}^{3,1}(\mathcal{T}_h)^3 : L_{\mathrm{bc},y}^{\mathrm{rod}}[w_h] = 0, \ y_h'(z) \cdot w_h'(z) = 0 \ \text{f.a. } z \in \mathcal{N}_h \}$$

while for a vector field $b_h \in \mathcal{S}^{1,0}(\mathcal{T}_h)^3$ we define

$$\mathcal{E}_h[b_h] = \{ v_h \in \mathcal{S}^{1,0}(\mathcal{T}_h)^3 : L_{\mathrm{bc},b}^{\mathrm{rod}}[v_h] = 0, \ v_h(z) \cdot b_h(z) = 0 \ \text{f.a. } z \in \mathcal{N}_h \}.$$

The functionals $L_{\mathrm{bc},y}^{\mathrm{rod}}$ and $L_{\mathrm{bc},b}^{\mathrm{rod}}$ are the components of $L_{\mathrm{bc}}^{\mathrm{rod}}$ corresponding to the variables y and b, respectively, assuming for simplicity that the boundary conditions can be appropriately separated.

We recall that the discretized functional with penalized orthogonality relation is defined as

$$I_{\mathrm{rod}}^{h,\varepsilon}[y_h, b_h] = \frac{\varkappa}{2} \int_0^L |y_h''|^2 \, dx + \frac{\theta}{2} \int_0^L |b_h'|^2 \, dx$$
$$- G_h[y_h, b_h] + P_{h,\varepsilon}[y_h, b_h] + N_h[y_h, b_h]$$

with the functionals

$$G_h[y_h, b_h] = \frac{\theta}{2} \int_0^L (Q_h b_h \cdot y_h'')^2 \, dx,$$

$$P_{h,\varepsilon}[y_h, b_h] = \frac{1}{2\varepsilon} \int_0^L \mathcal{I}_h^{1,0}[(y_h' \cdot b_h)^2] \, dx,$$

$$N_h[y_h, b_h] = \frac{1-\theta}{2} \int_0^L (b_h' \cdot (y_h' \times Q_h b_h))^2 \, dx$$

which are all *separately convex*, i.e., convex as functions in y_h for fixed b_h and vice versa.

Because of the requirement $0 < \theta \le \varkappa/2$, the functional $I_{\text{rod}}^{h,\varepsilon}$ is coercive on the set of functions (y_h, b_h) with $\|b_h\|_{L^\infty}^2 \le 3/2$. The nonlinear term N_h does not occur if $\varkappa \ge 2$. In this case the negative contribution in the energy functional $-G_h$ can be treated using its separate concavity properties. Otherwise, an inductive argument is used in the stability analysis which requires a different treatment. We generate a sequence $(y_h^k, b_h^k)_{k=0,1,...}$ that approximates a stationary configuration for $I_{\text{rod}}^{h,\varepsilon}$ using a discrete gradient flow that is determined by the metrics $(\cdot, \cdot)_\star$ and $(\cdot, \cdot)_\dagger$. These can be chosen quite general, however, our stability result relies on certain embeddings, see (7) below. To allow for an implicit or explicit treatment of some terms, depending on the value of $\varkappa$, we let

$$\widetilde{k} : \mathbb{N} \to \mathbb{N}_0$$

be either the identity $\widetilde{k}(k) = k$ or a negative shift $\widetilde{k}(k) = k - 1$, corresponding to an explicit or implicit treatment of the derivative of G_h with respect to b.

The *backward difference quotient* of a function a^k is $d_t a^k = \tau^{-1} (a^k - a^{k-1})$, which gives rise to the identity

$$2(a^k, d_t a^k) = d_t |a^k|^2 + \tau |d_t a^k|^2 \tag{6}$$

that will be used frequently.

Algorithm 1 (Gradient descent for elastic rods) Choose an initial pair $(y_h^0, b_h^0) \in \mathcal{A}_h$ and a step size $\tau > 0$, set $k = 1$.

(1) Compute $d_t y_h^k \in \mathcal{F}_h[y_h^{k-1}]$ such that for all $w_h \in \mathcal{F}_h[y_h^{k-1}]$ we have

$$(d_t y_h^k, w_h)_\star + \varkappa([y_h^k]'', w_h'') + \partial_y P_{h,\varepsilon}[y_h^k, b_h^{k-1}; w_h]$$
$$= \partial_y G_h[y_h^{k-1}, b_h^{k-1}; w_h] - \partial_y N_h[y_h^{k-1}, b_h^{k-1}; w_h].$$

(2) Compute $d_t b_h^k \in \mathcal{E}_h[b_h^{k-1}]$ such that for all $r_h \in \mathcal{E}_h[b_h^{k-1}]$ we have

$$(d_t b_h^k, r_h)_\dagger + \theta([b_h^k]', r_h') + \partial_b P_{h,\varepsilon}[y_h^k, b_h^k; r_h]$$
$$= \partial_b G_h[y_h^{\widetilde{k}}, b_h^{k-1}; r_h] - \partial_b N_h[y_h^{k-1}, b_h^{k-1}; r_h].$$

(3) Stop the iteration if $\|d_t y_h^k\|_\star + \|d_t b_h^k\|_\dagger \leq \varepsilon_{\text{stop}}$; otherwise, increase $k \to k+1$ and continue with (1).

Note that the N_h-terms on the right-hand sides vanish in case $\theta = 1$ which corresponds to $\varkappa \geq 2$.

It is useful to view $d_t y_h^k$ and $d_t b_h^k$ as the unknowns in Steps (1) and (2) instead of $y_h^k = y_h^{k-1} + \tau d_t y_h^k$ and $b_h^k = b_h^{k-1} + \tau d_t b_h^k$. The algorithm exploits the fact that the penalty term P_h is separately convex while $-G_h$, the nonquadratic contribution to the torsion term, is separately concave. Therefore, the decoupled semi-implicit treatment of these terms is natural and unconditionally energy stable if $\theta = 1$, i.e., in the bending-dominated case.

Proposition 2 (Convergent iteration) *Assume that we have*

$$\|w_h''\| \leq c_\star \|w_h\|_\star, \qquad \|r_h'\| \leq c_\dagger \|r_h\|_\dagger,$$
$$\|w_h'\|_{L^\infty} \leq c_\star \|w_h\|_\star, \quad \|r_h\|_{L^\infty} \leq c_\dagger \|r_h\|_\dagger \tag{7}$$

for all $(w_h, r_h) \in V_{\text{rod}}^h$ with $L_{\text{bc}}^{\text{rod}}[w_h, r_h] = 0$. For any $(y_h^0, b_h^0) \in V_{\text{rod}}^h$ there is a constant $c_0 \geq 0$ with the following property. Algorithm 1 is well defined and produces a sequence $(y_h^k, b_h^k)_{k=0,1,\dots}$ such that for all $L \geq 0$ with a constant $c_0 \geq 0$ we have

$$I_{\text{rod}}^{h,\varepsilon}[y_h^L, b_h^L] + \tau(1 - c_0\tau) \sum_{k=1}^{L} \left(\|d_t y_h^k\|_\star^2 + \|d_t b_h^k\|_\dagger^2 \right) \leq I_{\text{rod}}^{h,\varepsilon}[y_h^0, b_h^0],$$

for all $\tau \in (0, \tau_m)$ where

(a) $c_0 = 0$ and $\tau_m = \infty$ if $\theta = 1$ and $\widetilde{k} = k$,
(b) $c_0 > 0$ and $\tau_m = 1/(2c_0)$ if $\theta \leq 1$ and $\widetilde{k} = k - 1$.

In both cases, additionally assuming in (a) that $I_{\text{rod}}^{h,\varepsilon}[y_h^k, b_h^k] \geq 0$ for all $k = 0, 1, \dots, L$, the unit-length violation is controlled via

$$\max_{k=0,\dots,L} \left(\||[y_h^k]'|^2 - 1\|_{L^\infty} + \||b_h^k|^2 - 1\|_{L^\infty} \right) \leq \tau c_{\star,\dagger} e_{0,h},$$

where $e_{0,h} = I_{\text{rod}}^{h,\varepsilon}[y_h^0, b_h^0] < \infty$ and $c_{\star,\dagger} > 0$ only depends on the metrics.

Remark 1 In case $\theta = 1$ and $\widetilde{k} = k$, i.e., in case of low torsion rigidity, our stability result is conditional in the sense that we assume that the discrete energies remain nonnegative. In this case it suffices to require the second line of (7). Moreover, if we even replace it by $\|w_h'\| \leq c_\star \|w_h\|_\star$ and $\|r_h\| \leq c_\dagger \|r_h\|_\dagger$ the estimates for the constraint violation still hold in L^1 instead of L^∞.

In general, condition (7) can be satisfied if $\|\cdot\|_\star$ and $\|\cdot\|_\dagger$ are H^2- and H^1-seminorms and if $L_{\text{bc}}^{\text{rod}}$ imposes suitable Dirichlet conditions on one endpoint of the interval. An L^2-gradient flow, however, requires stronger assumptions on the step size.

Proof of Proposition 2 (a) We first consider the case $\theta = 1$ and $\widetilde{k} = k$ so that the nonlinearities related to the operator N_h disappear and the asserted estimate holds with $c_0 = 0$. For this we note that the functional G_h is separately convex, i.e., convex in y_h and in b_h. Therefore, we have that

$$\partial_y G_h[y_h^{k-1}, b_h^{k-1}; y_h^k - y_h^{k-1}] + G_h[y_h^{k-1}, b_h^{k-1}] \le G_h[y_h^k, b_h^{k-1}],$$
$$\partial_b G_h[y_h^k, b_h^{k-1}; b_h^k - b_h^{k-1}] + G_h[y_h^k, b_h^{k-1}] \le G_h[y_h^k, b_h^k],$$

which by summation leads to the inequality

$$\partial_y G_h[y_h^{k-1}, b_h^{k-1}; d_t y_h^k] + \partial_b G_h[y_h^k, b_h^{k-1}; d_t b_h^k] \le d_t G_h[y_h^k, b_h^k].$$

Similarly, the functional $P_{h,\varepsilon}$ is separately convex and we have

$$\partial_y P_{h,\varepsilon}[y_h^k, b_h^{k-1}; d_t y_h^k] + \partial_b P_{h,\varepsilon}[y_h^k, b_h^k; d_t b_h^k] \ge d_t P_{h,\varepsilon}[y_h^k, b_h^k].$$

We choose $w_h = d_t y_h^k$ and $r_h = d_t b_h^k$ in the equations of Steps (1) and (2) of Algorithm 1 and find that (using (6))

$$\|d_t y_h^k\|_\star^2 + \|d_t b_h^k\|_\dagger^2 + d_t \Big(\frac{\varkappa}{2} \|[y_h^k]''\|^2 + \frac{\theta}{2} \|[b_h^k]'\|^2 \Big) + d_t P_{h,\varepsilon}[y_h^k, b_h^k]$$
$$+ \tau \Big(\frac{\varkappa}{2} \|[d_t y_h^k]''\|^2 + \frac{\theta}{2} \|[d_t b_h^k]'\|^2 \Big)$$
$$\le \partial_y G_h[y_h^{k-1}, b_h^{k-1}; d_t y_h^k] + \partial_b G_h[y_h^k, b_h^{k-1}; d_t b_h^k] \le d_t G_h[y_h^k, b_h^k].$$

Since for $\theta = 1$ we have that

$$I_{\mathrm{rod}}^{h,\varepsilon}[y_h^k, b_h^k] = \frac{\varkappa}{2} \|[y_h^k]''\|^2 + \frac{1}{2} \|[b_h^k]'\|^2 - G_h[y_h^k, b_h^k] + P_{h,\varepsilon}[y_h^k, b_h^k]$$

we deduce the asserted estimate. The nodal orthogonality conditions encoded in the spaces $\mathcal{F}_h[y_h^{k-1}]$ and $\mathcal{E}_h[b_h^{k-1}]$ lead to the relations

$$|[y_h^k]'(z)|^2 = |[y_h^{k-1}]'(z)|^2 + \tau^2 |[d_t y_h^k]'(z)|^2,$$
$$|b_h^k(z)|^2 = |b_h^{k-1}(z)|^2 + \tau^2 |d_t b_h^k(z)|^2$$

for all $z \in \mathcal{N}_h$. Repeated application leads to

$$\Big\| |[y_h^k]'(z)|^2 - 1 \Big\|_{L^\infty} + \Big\| |b_h^k(z)|^2 - 1 \Big\|_{L^\infty} = \tau^2 \sum_{\ell=1}^k \Big(\|d_t b_h^\ell(z)\|_{L^\infty}^2 + \|[d_t y_h^\ell]'(z)\|_{L^\infty}^2 \Big).$$

Using (7) and the previously established bound for the discrete time derivatives proves the estimate for the constraint violation if $\theta = 1$ provided that the discrete energies $I_{\mathrm{rod}}^{h,\varepsilon}[y_h^k, b_h^k]$ remain nonnegative so that the right-hand side is controlled by the inital discrete energy.

(b) We next turn to the case $\theta \leq 1$ and $\widetilde{k} = k - 1$ and argue by induction over $L \geq 0$. Assume that the estimates have been established for some $\widetilde{L} = L - 1 \geq 0$ with $c_0 \geq c_{\star,\dagger} e_{0,h}$ (independent of L); the estimates trivially hold for $L = 0$. Let $0 \leq k \leq L$ and choose $w_h = d_t y_h^k$ and $r_h = d_t b_h^k$ in Algorithm 1. From $c_0 \tau \leq 1/2$ we infer

$$\|[y_h^{k-1}]'\|_{L^\infty}^2 \leq 3/2, \qquad \|b_h^{k-1}\|_{L^\infty}^2 \leq 3/2. \tag{8}$$

Since $0 < \theta \leq \varkappa/2$ and $\|Q_h r_h\|_{L^s} \leq \|r_h\|_{L^s}$, $1 \leq s \leq \infty$, the second estimate implies that

$$\left| G_h(y_h^{k-1}, b_h^{k-1}) \right| \leq \frac{3\varkappa}{8} \|[y_h^{k-1}]''\|^2. \tag{9}$$

In particular, we find the restricted coercivity bound

$$\frac{\varkappa}{8} \|[y_h^{k-1}]''\|^2 + \frac{\theta}{2} \|[b_h^{k-1}]'\|^2 \leq I_{\text{rod}}^{h,\varepsilon}[y_h^{k-1}, b_h^{k-1}] \leq e_{0,h}. \tag{10}$$

Arguing as above, i.e., choosing $w_h = d_t y_h^k$ and $r_h = d_t b_h^k$ in Algorithm 1, we find that

$$\|d_t y_h^k\|_\star^2 + \|d_t b_h^k\|_\dagger^2 + d_t \left\{ \frac{\varkappa}{2} \|[y_h^k]''\|^2 + \frac{\theta}{2} \|[b_h^k]'\|^2 + P_{h,\varepsilon}[y_h^k, b_h^k] \right\}$$
$$\leq G_h'[y_h^{k-1}, b_h^{k-1}; d_t y_h^k, d_t b_h^k] - N_h'[y_h^{k-1}, b_h^{k-1}; d_t y_h^k, d_t b_h^k]. \tag{11}$$

We note that

$$G_h'[y_h, b_h; w_h, r_h] = \theta \int_0^L (Q_h b_h \cdot y_h'') \left[Q_h b_h \cdot w_h'' + Q_h r_h \cdot y_h'' \right] \mathrm{d}x,$$

$$N_h'[y_h, b_h; w_h, r_h] = (1 - \theta) \int_0^L (b_h' \cdot (y_h' \times Q_h b_h)) \left[b_h' \cdot (w_h' \times Q_h b_h) \right.$$
$$\left. + r_h' \cdot (y_h' \times Q_h b_h) + b_h' \cdot (y_h' \times Q_h r_h) \right] \mathrm{d}x$$

and use Hölder inequalities, e.g., to bound

$$\left| G_h'[y_h, b_h; w_h, r_h] \right| \leq \theta \|Q_h b_h\|_{L^\infty}^2 \|y_h''\| \|w_h''\| + \theta \|Q_h b_h\|_{L^\infty} \|Q_h r_h\|_{L^\infty} \|y_h''\|^2.$$

Noting the inequalities (7) and the bounds (8) and (10) as well as the Young inequality we deduce that

$$\|d_t y_h^k\|_\star^2 + \|d_t b_h^k\|_\dagger^2 + d_t \left\{ \frac{\varkappa}{2} \|[y_h^k]''\|^2 + \frac{\theta}{2} \|[b_h^k]'\|^2 + P_{h,\varepsilon}[y_h^k, b_h^k] \right\}$$
$$\leq D_{0,h}' + \frac{1}{2} \left(\|d_t y_h^k\|_\star^2 + \|d_t b_h^k\|_\dagger^2 \right)$$

where $D'_{0,h}$ only depends on $\varkappa$, θ, and $e_{0,h}$, but in particular not on k. We consider the reduced energy functional

$$\widehat{I}^{h,\varepsilon}_{\mathrm{rod}}[y^k_h, b^k_h] = \frac{\varkappa}{2}\|[y^k_h]''\|^2 + \frac{\theta}{2}\|[b^k_h]'\|^2 + P_{h,\varepsilon}[y^k_h, b^k_h]$$

and note that because of (9) we have

$$\widehat{I}^{h,\varepsilon}_{\mathrm{rod}}[y^{k-1}_h, b^{k-1}_h] \le 4I^{h,\varepsilon}_{\mathrm{rod}}[y^{k-1}_h, b^{k-1}_h]. \tag{12}$$

We thus deduce from the estimate

$$\frac{1}{2}\left(\|d_t y^k_h\|^2_\star + \|d_t b^k_h\|^2_\dagger\right) + d_t \widehat{I}^{h,\varepsilon}_{\mathrm{rod}}[y^k_h, b^k_h] \le D'_{0,h}$$

that, imposing the condition $2c_0 \ge D'_{0,h}$ which implies $\tau D'_{0,h} \le 1$,

$$\frac{\tau}{2}\left(\|d_t y^k_h\|^2_\star + \|d_t b^k_h\|^2_\dagger\right) + \widehat{I}^{h,\varepsilon}_{\mathrm{rod}}[y^k_h, b^k_h] \le \tau D'_{0,h} + 4e_{0,h} \le 1 + 4e_{0,h} =: D_{0,h}.$$

This estimate and the unrestricted coercivity of $\widehat{I}^{h,\varepsilon}_{\mathrm{rod}}$ imply that

$$\|[y^k_h]''\| + \|[b^k_h]'\| \le D_{1,h}. \tag{13}$$

In the considered one-dimensional setting these bounds imply the L^∞ estimates

$$\|[y^k_h]'\|_{L^\infty} + \|b^k_h\|_{L^\infty} \le D'_{1,h}.$$

To obtain the asserted full energy law we find immediately from (11) that

$$\begin{aligned}
\|d_t y^k_h\|^2_\star + \|d_t b^k_h\|^2_\dagger + d_t I^{h,\varepsilon}_{\mathrm{rod}}[y^k_h, b^k_h] \\
\le d_t N_h[y^k_h, b^k_h] - N'_h[y^{k-1}_h, b^{k-1}_h; d_t y^k_h, d_t b^k_h] \\
- d_t G_h[y^k_h, b^k_h] + G'_h[y^{k-1}_h, b^{k-1}_h; d_t y^k_h, d_t b^k_h].
\end{aligned}$$

By the mean value theorem the terms on the right-hand side are equal to

$$\tau N''_h[\xi^{(1)}_h, \eta^{(1)}_h; d_t y^k_h, d_t b^k_h; d_t y^k_h, d_t b^k_h] - \tau G''_h[\xi^{(2)}_h, \eta^{(2)}_h; d_t y^k_h, d_t b^k_h; d_t y^k_h, d_t b^k_h],$$

where, e.g.,

$$\begin{aligned}
\partial_b \partial_y N[y_h, b_h; w_h, r_h] \\
= (1-\theta)\int_0^L \left(r'_h \cdot (y'_h \times Q_h b_h) + b'_h \cdot (y'_h \times Q_h r_h)\right)\left(b'_h \cdot (w'_h \times Q_h b_h)\right) \\
+ \left(b'_h \cdot (y'_h \times Q_h b_h)\right)\left(r'_h \cdot (w'_h \times Q_h b_h) + b'_h \cdot (w'_h \times Q_h r_h)\right) \mathrm{d}x.
\end{aligned}$$

The nodal values of $\xi_h^{(\ell)}$ and $\eta_h^{(\ell)}$, $\ell = 1, 2$, are convex combinations of y_h^{k-1} and y_h^k and b_h^{k-1} and b_h^k, respectively, and using their uniform bounds (8), (10), and (13) in combination with (7) we find that

$$\tau N_h''[\xi_h^{(1)}, \eta_h^{(1)}; d_t y_h^k, d_t b_h^k; d_t y_h^k, d_t b_h^k] \leq \tau c_{N''} D_{2,N} \big(\|d_t y_h^k\|_\star^2 + \|d_t b_h^k\|_\dagger^2\big),$$

$$\tau |G_h''[\xi_h^{(2)}, \eta_h^{(2)}; d_t y_h^k, d_t b_h^k; d_t y_h^k, d_t b_h^k]| \leq \tau c_{G''} D_{2,G} \big(\|d_t y_h^k\|_\star^2 + \|d_t b_h^k\|_\dagger^2\big).$$

With $c_0 \geq c_{N''} D_{2,N} + c_{G''} D_{2,G}$ we deduce the asserted estimate after multiplication by τ and summation over $k = 1, 2, \ldots, L$. The second estimate is established as in (a), provided the step size τ is bounded accordingly; the non-negativity of the discrete energy is guaranteed by (12). Note that all constants are formulated in terms of the initial discrete energy and generic constants related to parameters and functionals. Since the intermediate bound (13) is replaced by the bound (10) in the induction step, all estimates are re-initialized, and the condition on τ does not change with the number of induction steps. □

6 Experiments

Here we report on some numerical experiments. The parameters that have been used are shown in Table 1. The length of the curve is denoted by L, the number of nodes by N, the maximum step size $h_{\max}$ is normally close to L/N where L is the length of the curve. Except for Experiment 6.1, the initial curve has constant twist rate β_{ini}. While the director b will always be clamped on both ends of the rod, the boundary conditions (bc) for the curve are either periodic (p) or clamped on both ends (c). Unless otherwise stated the penalization parameter has been chosen to be $\varepsilon = \frac{2\pi}{N}$. We always use the time step size $\tau = \frac{1}{8} h_{\max}$. In some cases we also added some small perturbation to the initial curve which is specified in the text.

We briefly comment on the legend of the corresponding energy plots where the horizontal axis shows the iteration steps of the evolution. Of course, "bending" refers to the scaled bending energy $\frac{\varkappa}{2} \|y_h''\|_{L^2}^2$, "twisting" to the scaled twisting energy

Table 1 Modeling and discretization parameters for the experiments presented in Sect. 6

Section	L	N	$\varkappa$	β_{ini}	$h_{\max}$	ε	bc	ϱ
6.1	2π	100	2	*	0.0628	0.0628	c	–
6.2	2π	400	3/2	*	0.0157	10^{-5}	p	–
6.3	2π	400	2	5	0.0157	0.0010	p	–
6.4	$4K(m)$	400	*	0	0.0232	0.0232	p	–
6.5	*	400	2	4	0.0351	0.0010	c	–
6.6 (a)	2π	800	2	5	0.0079	0.0079	p	0.1
6.6 (b)	*	400	2	4	0.0351	0.0010	c	0.1

An asterisk refers to details given in the corresponding text

$\frac{\theta}{2} \left\| b'_h \right\|^2 - \frac{\theta}{2} \left\| Q_h b_h \cdot y''_h \right\|^2 + \frac{1-\theta}{2} \left\| b'_h \cdot (y'_h \times Q_h b_h) \right\|^2$ while "total twist" means the functional Tw defined in Sect. 2.4, "potential" to the tangent-point energy (see Sect. 6.6), "penalizing" to $P_{h,\varepsilon}$, and "total" is $I^{h,\varepsilon}_{rod}$.

In general the total twist is scaled differently, i.e., there is a second axis on the right margin of the energy plots while all other values refer to the axis on the left margin of the coordinate system. A coloring of a curve represents curvature values.

For typical discretizations with 400 nodes the overall runtime of our implementation in Matlab on a notebook (1.6 GHz DualCore, 8 GB RAM) took about $2\frac{1}{2}$ minutes per 10,000 iteration steps. An impermeable rod in Experiment 6.6, with an assembly of the self-avoidance potential in C, requires about 42 minutes per 10,000 iteration steps. For 800 nodes we observed a runtime of $6\frac{1}{2}$ minutes and almost three hours, respectively.

We would like to stress that we observe energy monotonicity for all our experiments, confirming the stability features discussed in Proposition 2. In particular, we did not observe difficulties related to negative energy values in the implicit case $k = \tilde{k}$.

6.1 Uniform twist rate

According to Sect. 2.6, stationary frames have constant twist rate. We expect that a non-uniform twist configuration will become constant within the evolution.

We start with a straight line curve of length 2π with uniform twist rate 4 on $[0, \frac{\pi}{2}]$ and 0 on $[\frac{\pi}{2}, 2\pi]$. No perturbation of the initial rod was used.

Initial stage and some intermediate steps from the evolution are visualized in Fig. 1. After 4000 steps the twist rate is nearly constant and amounts to 1.

All energy values are neglectable except for the twisting energy which virtually coincides with the total energy. Furthermore, at initial and final step the twisting energy data matchs quite closely the expected values of $\frac{1}{2} \int_0^{2\pi} \beta(s)^2 \, ds$ which amount to 4π and π.
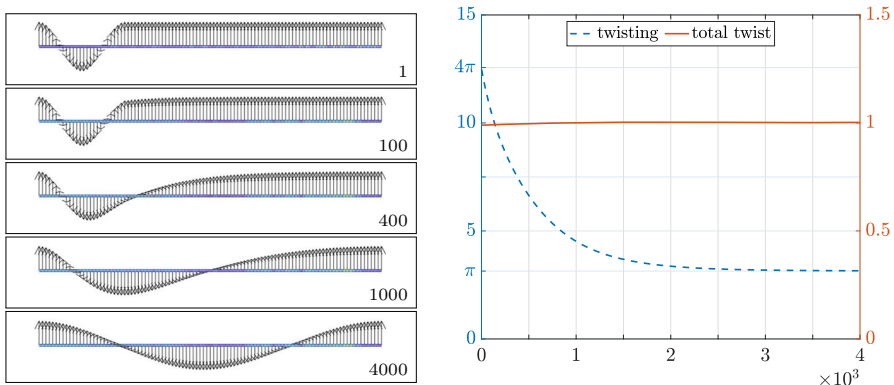
Fig. 1 (Experiment 6.1) Left—states of the evolution at several iteration steps. The initial rod consists of a straight line, framed with a non-uniform twist rate. Right—the twisting energy exhibits the dissipation of the twist rate after about 4000 iteration steps while the total twist is constant
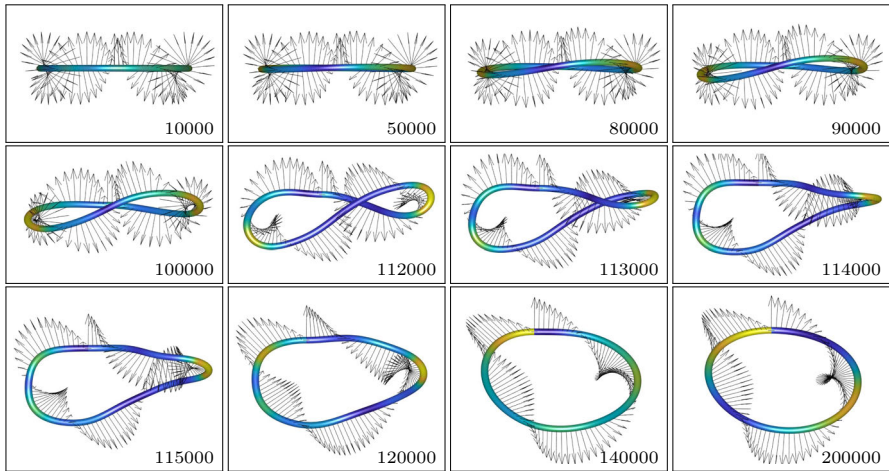
Fig. 2 In Experiment 6.2 we start the evolution with a round circle, framed with uniform twist rate $\beta_{\mathrm{ini}} = 4.2 > \beta_*$. The total twist is reduced by self-penetration in the course of the evolution around iteration step $k = 112{,}500$. It ends with another round circle, situated in a different plane

Looking at the following experiments whose initial configurations all have a uniform twist rate, we find this property being violated in the course of the iteration. In first place, this is due to the spatial behavior of the curve which does not seems to allow for an simultaneous reaction by the director. Eventually, uniform twist rate is restored, at least when the evolution has reached a stationary configuration, cf. Sect. 2.6.

We can test for uniform twist rate by computing the quotient of $\frac{2\pi^2}{L} \mathrm{Tw}^2$ over the twisting energy. As to Experiments 6.2 to 6.4, throughout the evolutions this number stays close to 1 for most of the time where we detect a relative deviation below $\frac{1}{200}$. The twist rate for Experiment 6.3 is plotted in Fig. 5 (right). In Experiment 6.4 we ignore the initial steps where the twist is zero. In the other cases, we also see that the twist rate eventually dissipates but it can last a relatively long time.

6.2 Michell's instability

We aim at experimentally confirming Zajac's threshold $\beta_* = 2\pi\sqrt{3}\varkappa/L$, see Sect. 2.8.

We consider the initial curve $y(s) = (\cos s, \sin s, 0)^\top$ with the director

$$b(s) = \cos(\beta_{\mathrm{ini}} s) \begin{pmatrix} -\cos s \\ -\sin s \\ 0 \end{pmatrix} + \sin(\beta_{\mathrm{ini}} s) \begin{pmatrix} 0 \\ 0 \\ 1 \end{pmatrix}, \qquad s \in [0, 2\pi].$$

In order to break symmetry which seems to prevent rod configurations from leaving even energetically unfavorable states, a slight perturbation has been applied to the initial curve, namely

$$s \mapsto \tfrac{1}{1000} \sin(7s) \tag{14}$$
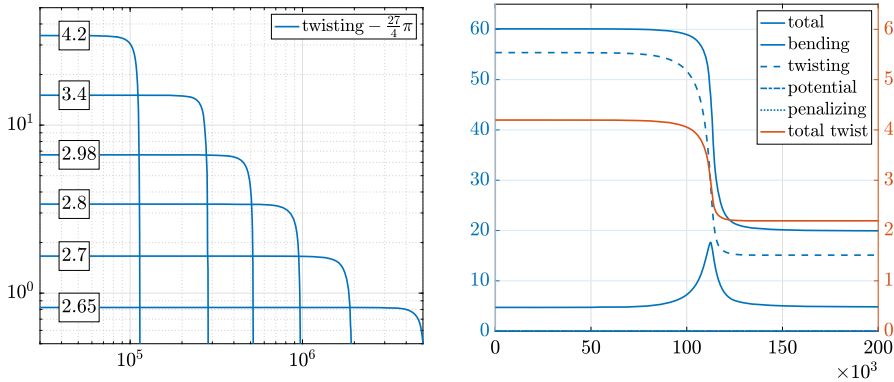
Fig. 3 (Experiment 6.2) Left—in order to experimentally confirm Zajac's threshold, we repeat the evolution depicted in Fig. 2 above for different twist rates $\beta_{\text{ini}} > \beta_*$. The evolutions turn out to be very similar; essentially they only differ in speed. The (logarithmically scaled) twisting profiles reveal a drastic reduction of the twisting energy (due to the self-penetration of the curve). The smallest iteration step at which the twisting energy is below $\frac{27}{4}\pi$ serves as a threshold for the speed of the evolution. Right—the energy plot for the evolution from Fig. 2 where $\beta_{\text{ini}} = 4.2$. Here the twisting energy decay occurs around iteration step 114,200

perpendicularly to the plane (i.e., in z-direction); the frame is corrected accordingly.

In order to quantitatively verify Zajac's threshold, we had to choose a rather high penalty coefficient, namely $\varepsilon = 10^{-5}$. For $\varkappa = 3/2$, we obtain

$$\beta_* = \tfrac{3}{2}\sqrt{3} \approx 2.5981.$$

In Fig. 3 (left) we plot the twisting energy of several evolutions using logarithmic scales on both axes. From top to bottom, the profiles correspond to initial values of $\beta_{\text{ini}} = \beta_* + \frac{2^\ell}{10}$ for $\ell = -1, 0, 1, 2, 3, 4$. More precisely, we plot the twisting energy of the evolutions corresponding to different values of β_{ini} minus the twisting energy of the configuration at β_*, i.e., $\frac{1}{2}\int_0^{2\pi}\beta(s)^2\,\mathrm{d}s - \frac{27}{4}\pi$, which seems to be stationary. Of course, values less than $\frac{27}{4}\pi \approx 21.2058$ are ignored.

Experimentally we find that evolutions for different initial values of β_{ini} seem to be very similar and essentially only vary in speed. The region of iteration steps where the twisting energy drastically falls is a good indication for the latter. There is one caveat—probably due to symmetry it turned out that the evolution corresponding to the initial values $\beta_{\text{ini}} = 3$ is remarkably slower than expected. Therefore we chose $\beta_{\text{ini}} = 2.98$ instead.

The plot in Fig. 3 (left) indicates a reciprocal dependence of the evolution speed on $\beta_{\text{ini}} - \beta_*$. For values $\beta_{\text{ini}} \leq \beta_*$ the initial configuration remained unchanged (at least until step $k = 5 \cdot 10^6$). This confirms Zajac's threshold as desired.

We show a typical full energy profile in Fig. 3 (right) for the initial value $\beta_{\text{ini}} = 4.2$. Some iteration steps are visualized in Fig. 2. The corresponding plots for the other initial values of β_{ini} essentially differ by the scaling of the horizontal axis and the simulations looks very similar. Initial and final stage are round circles which
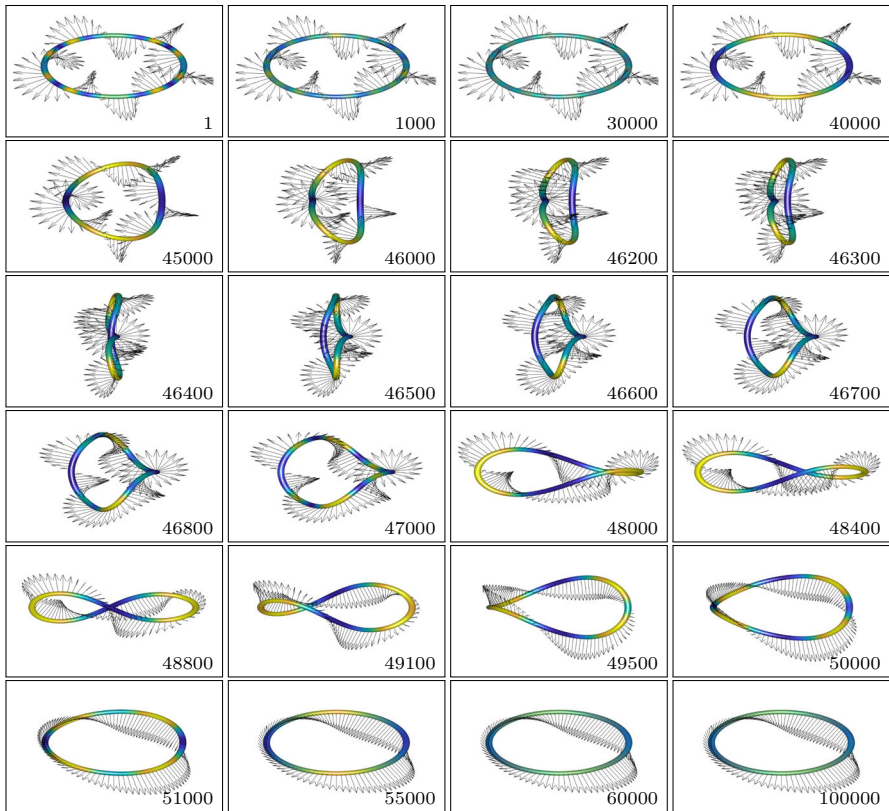
Fig. 4 Evolution of a round circle twisted by five full rotations in Experiment 6.3. Twist is reduced due to self-penetrations of the rod around iteration steps $k = 46{,}400$ and $k = 48{,}800$. Initial and final curves are round circles which appear to lie in the same plane. Plots of energy profile and twist rate are shown in Fig. 5 below

correspond to the (unique) global bending energy minimum of $L = 2\pi$ among all closed curves.

Note that the total twist is reduced by precisely 2 from $\beta_{\text{ini}} = 4.2$ to $\beta = 2.2$. In light of Sect. 2.7 a second reduction would be possible as well. However, in contrast to Experiment 6.3 below, the gradient of the energy does not seem to be steep enough to invest the amount of additional bending required for another self-penetration. As $2.2 < \beta_*$ the evolution becomes stationary due to Michell's instability.

6.3 Reducing twist by self-penetration

We repeat the experiment from Sect. 6.2 with $\varkappa = 2$ and $\beta_{\text{ini}} = 5$, i.e., for a continuous frame. Here we have $\beta_* \approx 3.4641$. The same slight perturbation has been added to the initial curve as before in (14).

In this case we observe twist reduction by two consecutive self-penetrations although the evolution could possibly stop after the first one since the twist value
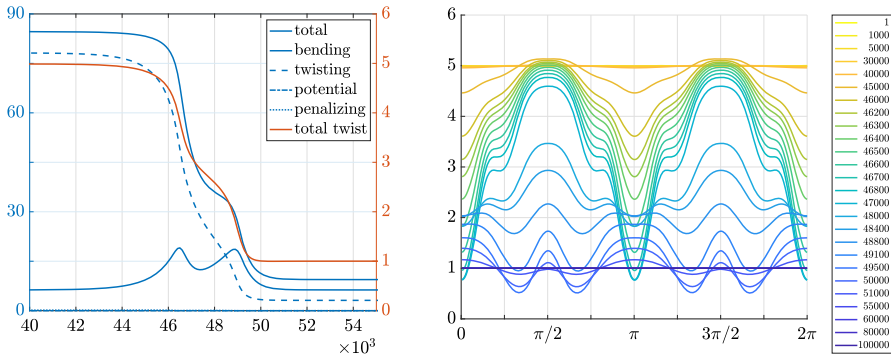
Fig. 5 (Experiment 6.3) Left—the energy plot reveals two peaks of the bending profile corresponding to the two self-penetrations. The energy profile is virtually constant for the iteration steps outside the range shown here. Right—plot of the twist rate β for the iteration steps visualized in Fig. 4. Apart from the initial configuration, the twist rate is non-uniform throughout the evolution. It eventually dissipates around iteration step 100,000
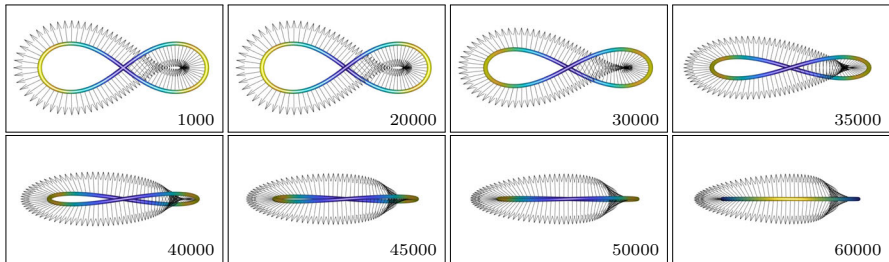
Fig. 6 Evolution of a twist-free planar elastic figure eight from Experiment 6.4 with $\varkappa = 0.7$. The initial curve is (almost) planar and evolves to a circle in a plane which seems to be perpendicular to the initial configuration. The corresponding frame performs one full rotation. Obviously the bending forces dominate in this case. The energy plot is shown in Fig. 7 (right)

is then already below the threshold β_*. Obviously, the gradient of the energy of the noncircular configuration around iteration step $k = 48{,}000$ is so steep that Michell's instability does not play any role here.

The evolution is visualized in Fig. 4 and the energy values are plotted in Fig. 5 (left). As the initial and final configurations are circular and the frame closes up (because of $\beta_{\text{ini}} \in \mathbb{Z}$), the total twist is integer at the beginning and end of the evolution (cf. Sect. 2.4).

The twist rate, however, does not stay uniform throughout the evolution as can be seen from Fig. 5 (right). Eventually the twist will be balanced similarly to Experiment 6.1.

6.4 Planar figure eight

Any closed *planar* elastica (i.e., a critical point of the bending energy) is either a circle or a planar figure-eight curve, possibly several times covered, cf. Sachkov [61].
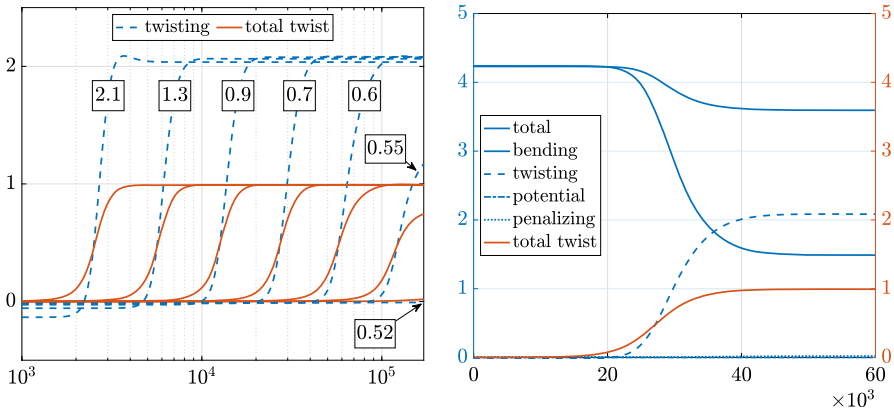
Fig. 7 (Experiment 6.4) Left—aiming at experimentally confirming the threshold $\varkappa = \frac{1}{2}$, we study (semi-logarithmically scaled) profiles of twisting energy and total twist for several evolutions of the figure-eight curve. The smallest iteration step at which the total twist is above $\frac{1}{2}$ serves as a threshold for the speed of the evolution. Right—energy plot for the evolution in Fig. 6 where $\varkappa = 0.7$

Explicit formulae for elastica based on special functions have been computed in the 19th century, see the references in Levien [43]. Here we make use of an arclength parametrization given by Dall'Acqua and Pluda [21] which relies on earlier work by Djondjorov et al. [24], namely

$$y(s) = \begin{pmatrix} 2E(\mathrm{am}(s, m), m) - s \\ 2\sqrt{m}\,\mathrm{cn}(s, m) \end{pmatrix}, \qquad s \in \mathbb{R}/4K(m)\mathbb{Z}.$$

Here E denotes the incomplete elliptic integral of the second kind and K the complete elliptic integral of the first kind while am is the Jacobi amplitude function and cn the elliptic cosine function, cf. [21]. The (signed) curvature amounts to $s \mapsto -2\sqrt{m}\,\mathrm{cn}(s, m)$. The figure-eight curve corresponds to $m \approx 0.82611$ which is the uniquely defined number in $(0, 1)$ with $2E(\frac{\pi}{2}, m) = K(m) \approx 2.321$.

In order to break the symmetry which may result in an unstably stationary configuration, a slight perturbation similarly to (14) has been added to the initial curve, namely $s \mapsto \frac{1}{1000} \sin\left(7 \cdot \frac{2\pi}{4K(m)} s\right)$, perpendicularly to the plane (i.e., in z-direction); the frame is corrected accordingly.

According to Ivey and Singer [37, Sect. 7] the twist-free planar figure-eight is stable if $\varkappa = c_{\mathrm{b}}/c_{\mathrm{t}} < \frac{1}{2}$ and unstable if $\varkappa > \frac{1}{2}$.

We performed several evolutions whose energy plots are depicted in Fig. 7 (left). As in Experiment 6.2, the evolutions are very similar and essentially only differ in speed. In each case the total twist is raised from zero to one which is still in accordance with the bound $|\mathrm{Tw}| \leq 1$ in Sect. 2.7. Mind the semi-logarithmic scaling of the horizontal axis. Negative values of the twisting energy are due to discretization errors and tend to zero when choosing a larger number of nodes.

Snapshots of the evolution for $\varkappa = 0.7$ can be found in Fig. 6. We observe an evolution to a round circle with one full twist. For the same reason as in Experiment 6.3
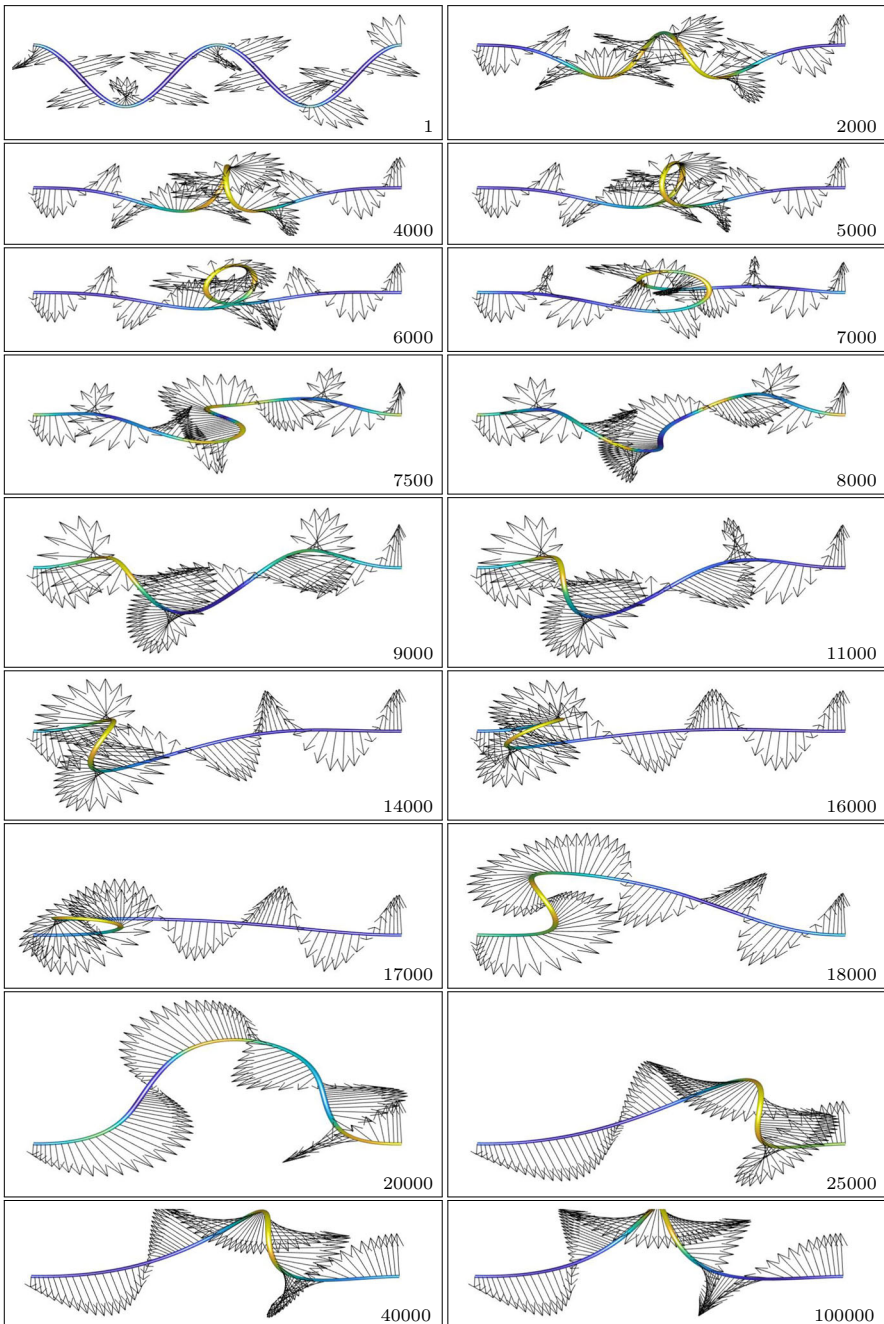
Fig. 8 Evolution of an open clamped rod from Experiment 6.5. The total twist amounts to 8 initially and is then reduced to about 2 by two self-penetrations which occur around iteration steps 6000 and 16,500. The energy plot is shown in Fig. 9 below

Fig. 9 Energy plot for the evolution from Experiment 6.5. Reduction of twist occurs following the self-penetrations of the curve. Total twist attains the values of 5 and 3 around iteration steps 7200 and 18,800 respectively. The energy profile is virtually constant for the iteration steps $\geq 30{,}000$
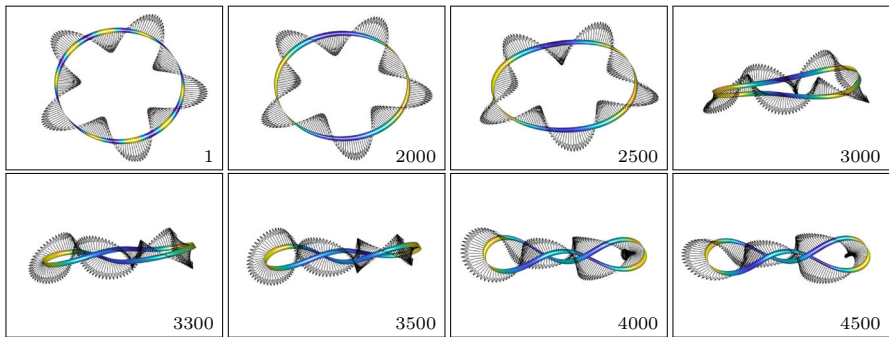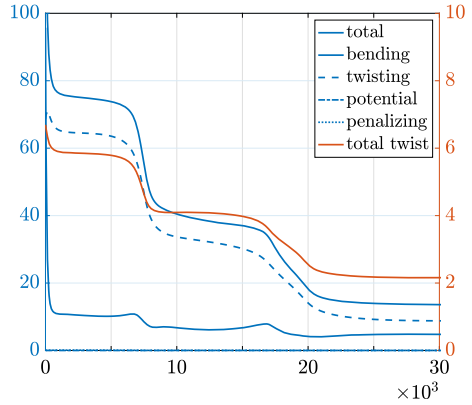
Fig. 10 In the first part of Experiment 6.6 we repeat Experiment 6.3 in the presence of impermeability. As self-penetrations are excluded, we observe the formation of coilings. The energy plot is shown in Fig. 12 (left)

we face integer values of Tw at beginning and end of the evolution. The full energy plot is depicted in Fig. 7 (right).

The parameters $\varkappa$ of the profiles shown in Fig. 7 (left) amount to $\varkappa = \frac{1}{2} + \frac{2^\ell}{10}$ for $\ell = -2, -1, 0, 1, 2, 3, 4$. The red solid line corresponding to $\varkappa = 0.52$ is just about to lift at the right margin. The speed of the evolution seems to reciprocally depend on $\varkappa - \frac{1}{2}$, suggesting that the evolutions for $\varkappa \leq \frac{1}{2}$ will be stationary. This confirms the threshold by Ivey and Singer as desired.

6.5 Open clamped rods

We can also simulate the evolution of *open* rods. Our initial curve is planar, namely

$$y(s) = \begin{pmatrix} \frac{1}{2}s \\ \cos s - 1 \end{pmatrix}, \qquad s \in [0, 4\pi].$$
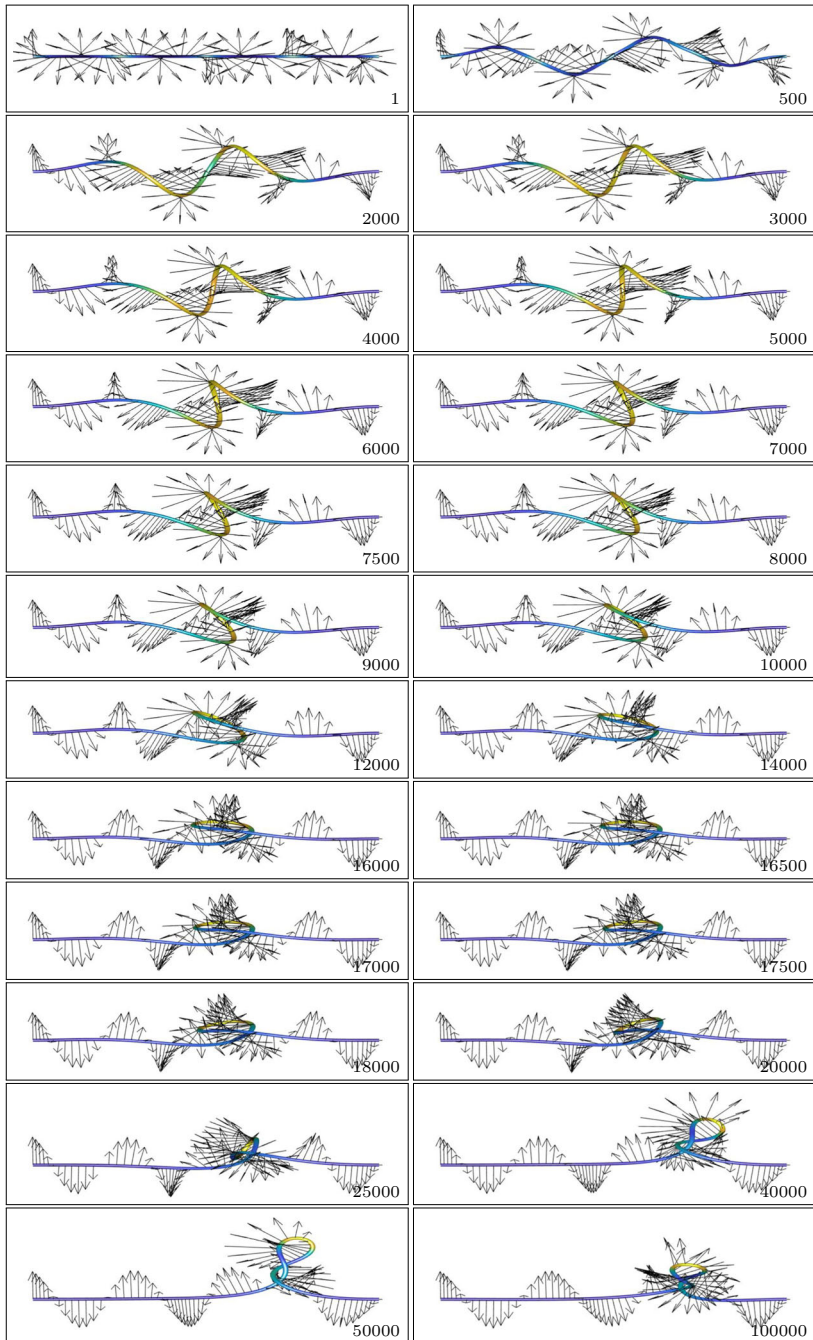
Fig. 11 In the second part of Experiment 6.6 we repeat Experiment 6.5 in the presence of impermeability. As self-penetrations are excluded, we observe the formation of a plectoneme. The viewer's position has been rotated by 90°. The energy plot is shown in Fig. 12 (right)

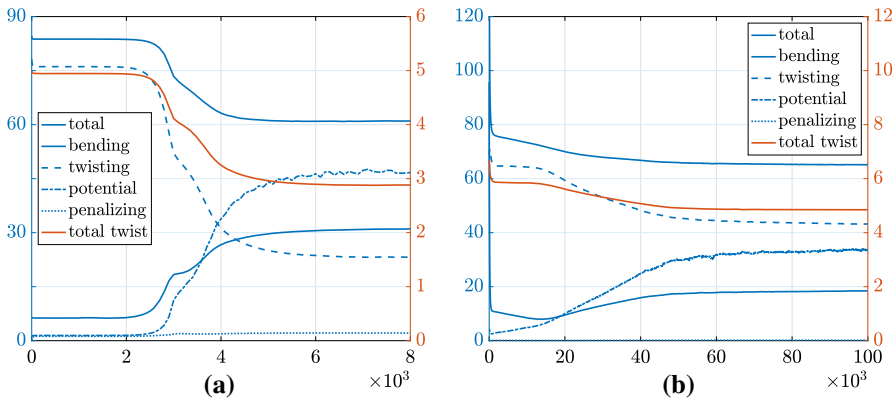**Fig. 12** Energy plots for Experiment 6.6 (**a**) and (**b**)

This curve is not parametrized by arclength, with the notation of elliptic integrals introduced in Experiment 6.4 we have $L = 4\sqrt{2}E(\frac{\pi}{2}, -2) \approx 12.357$. No perturbation of the initial rod was used.

Choosing $\beta_{\text{ini}} = 4$ gives an initial total twist of 8 according to Sect. 2.4.

The evolution is depicted in Fig. 8, the corresponding energy plot can be found in Fig. 9. It seems to become stationary after 30,000 steps although the total twist could be further reduced, see Sect. 2.7 (Figs. 10, 11).

6.6 Implementing impermeability

In order to preclude rods from self-penetrations we consider the modified total energy $I_{\text{rod}} + \varrho\text{TP}$ where $\varrho \geq 0$ and TP denote the *tangent-point functional*

$$y \mapsto \frac{1}{2^q q} \int_0^L \int_0^L \frac{\mathrm{d}s\,\mathrm{d}\tilde{s}}{r(y(\tilde{s}), y(s))^q}, \qquad q > 2. \qquad (15)$$

Here $s, \tilde{s}$ denotes arclength parameters, and $r(y(\tilde{s}), y(s))$ is the radius of the circle that is tangent to y at the point $y(\tilde{s})$ and that intersects with y in $y(s)$.

As many so-called knot energies [56], the tangent-point energies provide a monotonic uniform bound on the bi-Lipschitz constant. This implies in particular that the energy values of a sequence of embedded curves converging to a curve with a self-intersection will necessarily blow up.

The tangent-point energies have been proposed by Gonzalez and Maddocks [27]; the scale invariant case $q = 2$ has already been introduced by Buck and Orloff [11]. They are defined on (smooth) embedded curves $y : [0, L] \to \mathbb{R}^n$ and take values in $[0, +\infty]$, see Strzelecki and von der Mosel [70] and references therein. Blatt [9] has characterized the energy spaces in terms of Sobolev–Slobodeckiĭ spaces; regularity aspects are discussed in [10].

More information on the discretization of the tangent-point functional can be found in [6,7]. We cut out a strip of radius $2h_{\text{max}}$ off the diagonal in $[0, L]^2$.

We repeat Experiments 6.3 and 6.5 in the presence of self-avoidance. No perturbation was added to the initial curves. The parameters are chosen similarly, see Table 1.

Note that for closed curves with a closed frame the linking number is preserved throughout the evolution. Changes of the total twist will be entirely compensated by the writhe functional.

References

1. Antman, S.S.: Nonlinear Problems of Elasticity, Volume 107 of Applied Mathematical Sciences, 2nd edn. Springer, New York (2005)
2. Arunakirinathar, K., Reddy, B.D.: Mixed finite element methods for elastic rods of arbitrary geometry. Numer. Math. **64**(1), 13–43 (1993)
3. Barrett, J.W., Garcke, H., Nürnberg, R.: Parametric approximation of isotropic and anisotropic elastic flow for closed and open curves. Numer. Math. **120**(3), 489–542 (2012)
4. Bartels, S.: A simple scheme for the approximation of the elastic flow of inextensible curves. IMA J. Numer. Anal. **33**(4), 1115–1125 (2013)
5. Bartels, S.: Finite Element Simulation of Nonlinear Bending Models for Thin Elastic Rods and Plates. Handbook of Numerical Analysis. Elsevier, Amsterdam (2019)
6. Bartels, S., Reiter, Ph.: Stability of a simple scheme for the approximation of elastic knots and self-avoiding inextensible curves. arXiv e-prints (2018)
7. Bartels, S., Reiter, Ph., Riege, J.: A simple scheme for the approximation of self-avoiding inextensible curves. IMA J. Numer. Anal. drx021 (2017)
8. Bergou, M., Wardetzky, M., Robinson, S., Audoly, B., Grinspun, E.: Discrete elastic rods. ACM Trans. Graph. **27**(3), 63:1–63:12 (2008)
9. Blatt, S.: The energy spaces of the tangent point energies. J. Topol. Anal. **5**(3), 261–270 (2013)
10. Blatt, S., Reiter, Ph: Regularity theory for tangent-point energies: the non-degenerate sub-critical case. Adv. Calc. Var. **8**(2), 93–116 (2015)
11. Buck, G., Orloff, J.: A simple energy function for knots. Topol. Appl. **61**(3), 205–214 (1995)
12. Călugăreanu, G.: L'intégrale de Gauss et l'analyse des nœuds tridimensionnels. Rev. Math. Pures Appl. **4**, 5–20 (1959)
13. Călugăreanu, G.: Sur les classes d'isotopie des nœuds tridimensionnels et leurs invariants. Czechoslovak Math. J. **11**(86), 588–625 (1961)
14. Clauvelin, N., Audoly, B., Neukirch, S.: Matched asymptotic expansions for twisted elastic knots: a self-contact problem with non-trivial contact topology. J. Mech. Phys. Solids **57**(9), 1623–1656 (2009)
15. Coleman, B.D., Dill, E.H., Lembo, M., Lu, Z., Tobias, I.: On the dynamics of rods in the theory of Kirchhoff and Clebsch. Arch. Ration. Mech. Anal. **121**(4), 339–359 (1992)
16. Coleman, B.D., Swigon, D.: Theory of supercoiled elastic rings with self-contact and its application to DNA plasmids. J. Elast. **60**(3), 173–221 (2001)

17. Coleman, B.D., Swigon, D.: Theory of self-contact in Kirchhoff rods with applications to supercoiling of knotted and unknotted DNA plasmids. Philos. Trans. R. Soc. Lond. Ser. A Math. Phys. Eng. Sci. **362**(1820), 1281–1299 (2004)
18. Coleman, B.D., Swigon, D., Tobias, I.: Elastic stability of DNA configurations. II. Supercoiled plasmids with self-contact. Phys. Rev. E (3) **61**(1), 759–770 (2000)
19. da Costa e Silva, C., Maassen, S.F., Pimenta, P.M., Schröder, J.: A simple finite element for the geometrically exact analysis of Bernoulli–Euler rods. Comput. Mech. **65**(4), 905–923 (2020)
20. Dall'Acqua, A., Lin, C.-C., Pozzi, P.: Evolution of open elastic curves in $\mathbb{R}^n$ subject to fixed length and natural boundary conditions. Analysis (Berlin) **34**(2), 209–222 (2014)
21. Dall'Acqua, A., Pluda, A.: Some minimization problems for planar networks of elastic curves. Geom. Flows **2**(1), 105–124 (2017)
22. Deckelnick, K., Dziuk, G.: Error analysis for the elastic flow of parametrized curves. Math. Comp. **78**(266), 645–671 (2009)
23. Dichmann, D.J., Li, Y., Maddocks, J.H.: Hamiltonian formulations and symmetries in rod mechanics. In: Mathematical approaches to biomolecular structure and dynamics (Minneapolis, MN, 1994), volume 82 of IMA Vol. Mathematical Applications, pp. 71–113. Springer, New York (1996)
24. Djondjorov, P.A., Hadzhilazova, M.T., Mladenov, I.M., Vassilev, V.M.: Explicit Parameterization of Euler's Elastica. Geometry, Integrability and Quantization, pp. 175–186. Softex, Sofia (2008)
25. Dziuk, G., Kuwert, E., Schätzle, R.: Evolution of elastic curves in $\mathbb{R}^n$: existence and computation. SIAM J. Math. Anal. **33**(5), 1228–1245 (2002)
26. Gerlach, H., Reiter, Ph, von der Mosel, H.: The elastic trefoil is the doubly covered circle. Arch. Ration. Mech. Anal. **225**(1), 89–139 (2017)
27. Gonzalez, O., Maddocks, J.H.: Global curvature, thickness, and the ideal shapes of knots. Proc. Natl. Acad. Sci. USA **96**(9), 4769–4773 (1999)
28. Gonzalez, O., Maddocks, J.H., Schuricht, F., von der Mosel, H.: Global curvature and self-contact of nonlinearly elastic curves and rods. Calc. Var. Partial Differ. Equ. **14**(1), 29–68 (2002)
29. Goriely, A.: Twisted elastic rings and the rediscoveries of Michell's instability. J. Elast. **84**(3), 281–299 (2006)
30. Goriely, A., Tabor, M.: Nonlinear dynamics of filaments. I. Dynamical instabilities. Phys. D **105**(1–3), 20–44 (1997a)
31. Goriely, A., Tabor, M.: Nonlinear dynamics of filaments. II. Nonlinear analysis. Phys. D **105**(1–3), 45–61 (1997b)
32. Goyal, S., Perkins, N., Lee, C.: Non-linear dynamic intertwining of rods with self-contact. Int. J. Non-Linear Mech. **43**(1), 65–73 (2008). cited By 34
33. Goyal, S., Perkins, N.C., Lee, C.L.: Nonlinear dynamics and loop formation in Kirchhoff rods with implications to the mechanics of DNA and cables. J. Comput. Phys. **209**(1), 371–389 (2005)
34. Hoffman, K.A., Seidman, T.I.: A variational characterization of a hyperelastic rod with hard self-contact. Nonlinear Anal. **74**(16), 5388–5401 (2011a)
35. Hoffman, K.A., Seidman, T.I.: A variational rod model with a singular nonlocal potential. Arch. Ration. Mech. Anal. **200**(1), 255–284 (2011b)
36. Hu, K.: Buckling of some isotropic, intrinsically curved elastics induced by a terminal twist. Appl. Math. Lett. **16**(2), 193–197 (2003)
37. Ivey, T.A., Singer, D.A.: Knot types, homotopies and stability of closed elastic rods. Proc. Lond. Math. Soc. (3) **79**(2), 429–450 (1999)
38. Kehrbaum, S., Maddocks, J.H.: Elastic rods, rigid bodies, quaternions and the last quadrature. Philos. Trans. R. Soc. Lond. Ser. A **355**(1732), 2117–2136 (1997)
39. Krömer, S., Valdman, J.: Global injectivity in second-gradient nonlinear elasticity and its approximation with penalty terms. Math. Mech. Solids **24**(11), 3644–3673 (2019)
40. Langer, J., Singer, D.A.: Curve straightening and a minimax argument for closed elastic curves. Topology **24**(1), 75–88 (1985)
41. Langer, J., Singer, D.A.: Lagrangian aspects of the Kirchhoff elastic rod. SIAM Rev. **38**(4), 605–618 (1996)
42. Le Tallec, P., Mani, S., Rochinha, F.A.: Finite element computation of hyperelastic rods in large displacements. RAIRO Modél. Math. Anal. Numér. **26**(5), 595–625 (1992)
43. Levien, R.: The elastica: a mathematical history. Technical Report UCB/EECS-2008-103, EECS Department, University of California, Berkeley (2008)

44. Lin, C.-C., Schwetlick, H.R.: On the geometric flow of Kirchhoff elastic rods. SIAM J. Appl. Math. **65**(2), 720–736 (2004)
45. Maddocks, J.H.: Bifurcation theory, symmetry breaking and homogenization in continuum mechanics descriptions of DNA. Mathematical modelling of the physics of the double helix. In: A Celebration of Mathematical Modeling, pp. 113–136. Kluwer, Dordrecht (2004)
46. Manhart, A., Oelz, D., Schmeiser, C., Sfakianakis, N.: An extended filament based lamellipodium model produces various moving cell shapes in the presence of chemotactic signals. J. Theor. Biol. **382**, 244–258 (2015)
47. Manning, R.S., Maddocks, J.H.: Symmetry breaking and the twisted elastic ring. Comput. Methods Appl. Mech. Eng. **170**(3–4), 313–330 (1999). Computational methods and bifurcation theory with applications
48. Manning, R.S., Rogers, K.A., Maddocks, J.H.: Isoperimetric conjugate points with application to the stability of DNA minicircles. R. Soc. Lond. Proc. Ser. A Math. Phys. Eng. Sci. **454**(1980), 3047–3074 (1998)
49. Meier, C., Popp, A., Wall, W.A.: An objective 3D large deformation finite element formulation for geometrically exact curved Kirchhoff rods. Comput. Methods Appl. Mech. Eng. **278**, 445–478 (2014)
50. Michell, J.H.: On the stability of a bent and twisted wire. *Messenger Math.* 11, 181–184; 1889–1890. Reprinted in [29]
51. Moffatt, H.K., Ricca, R.L.: Helicity and the Călugăreanu invariant. Proc. R. Soc. Lond. Ser. A **439**(1906), 411–429 (1992)
52. Mora, M.G., Müller, S.: Derivation of the nonlinear bending-torsion theory for inextensible rods by Γ-convergence. Calc. Var. Partial Differ. Equ. **18**(3), 287–305 (2003)
53. Needham, T.: Kähler structures on spaces of framed curves. Ann. Glob. Anal. Geom. **54**(1), 123–153 (2018)
54. Neukirch, S., Henderson, M.E.: Classification of the spatial equilibria of the clamped elastica: symmetries and zoology of solutions. J. Elast. **68**(1–3), 95–121 (2003)
55. O'Hara, J.: Family of energy functionals of knots. Topol. Appl. **48**(2), 147–161 (1992)
56. O'Hara, J.: Energy of Knots and Conformal Geometry. Series on Knots and Everything, Vol. 33. World Scientific, River Edge (2003)
57. Pozzi, P., Stinner, B.: Curve shortening flow coupled to lateral diffusion. Numer. Math. **135**(4), 1171–1205 (2017)
58. Ranner, T.: A stable finite element method for low inertia undulatory locomotion in three dimensions. arXiv e-prints (2019)
59. Reiter, Ph: Repulsive knot energies and pseudodifferential calculus for O'Hara's knot energy family $E^{(\alpha)}$, $\alpha \in [2, 3)$. Math. Nachr. **285**(7), 889–913 (2012)
60. Romero, I.: The interpolation of rotations and its application to finite element models of geometrically exact rods. Comput. Mech. **34**(2), 121–133 (2004)
61. Sachkov, Y.L.: Closed Euler elasticae. Proc. Steklov Inst. Math. **278**(1), 218–232 (2012)
62. Sander, O.: Geodesic finite elements for Cosserat rods. Int. J. Numer. Methods Eng. **82**(13), 1645–1670 (2010)
63. Scholtes, S., Schumacher, H., Wardetzky, M.: Variational Convergence of Discrete Elasticae. arXiv e-prints (2019)
64. Schuricht, F., von der Mosel, H.: Euler–Lagrange equations for nonlinearly elastic rods with self-contact. Arch. Ration. Mech. Anal. **168**(1), 35–82 (2003)
65. Spillmann, J., Teschner, M.: An adaptive contact model for the robust simulation of knots. Comput. Graph. Forum **27**(2), 497–506 (2008)
66. Starostin, E.L.: Symmetric equilibria of a thin elastic rod with self-contacts. Philos. Trans. R. Soc. Lond. Ser. A Math. Phys. Eng. Sci. **362**, 1317–1334 (1820), 2004
67. Starostin, E.L., van der Heijden, G.H.M.: Theory of equilibria of elastic 2-braids with interstrand interaction. J. Mech. Phys. Solids **64**, 83–132 (2014a)
68. Starostin, E.L., van der Heijden, G.H.M.: Tightening elastic $(n, 2)$-torus knots. J. Phys. Conf. Ser. **544**(1), 012007 (2014b)
69. Starostin, E.L., van der Heijden, G.H.M.: Equilibria of elastic cable knots and links. In: Blatt, S., Reiter, Ph, Schikorra, A. (eds.) New Directions in Geometric and Applied Knot Theory, pp. 258–275. De Gruyter, Berlin (2018)
70. Strzelecki, P., von der Mosel, H.: Tangent-point self-avoidance energies for curves. J. Knot Theory Ramif. **21**(5), 1250044-28 (2012)

71. Tobias, I., Coleman, B.D., Lembo, M.: A class of exact dynamical solutions in the elastic rod model of DNA with implications for the theory of fluctuations in the torsional motion of plasmids. J. Chem. Phys. **105**(6), 2517–2526 (1996)
72. Tobias, I., Olson, W.K.: The effect of intrinsic curvature on supercoiling: predictions of elasticity theory. Biopolymers **33**(4), 639–646 (1993)
73. Tobias, I., Swigon, D., Coleman, B.D.: Elastic stability of DNA configurations. I. General theory. Phys. Rev. E (3) **61**(1), 747–758 (2000)
74. van der Heijden, G., Neukirch, S., Goss, V., Thompson, J.: Instability and self-contact phenomena in the writhing of clamped rods. Int. J. Mech. Sci. **45**(1), 161–196 (2003)
75. von der Mosel, H.: Minimizing the elastic energy of knots. Asymptot. Anal. **18**(1–2), 49–65 (1998)
76. Zajac, E.E.: Stability of two planar loop elasticas. Trans. ASME Ser. E. J. Appl. Mech. **29**, 136–142 (1962)